Development of Laser Powder Bed Fusion NASA HR-2 for Hydrogen Sensitive Liquid Rocket Engine Applications

Po S. Chen[1]
Amentum Space Exploration Group, NASA Marshall Space Flight Center, Huntsville, AL 35812

Benjamin L. Rupp[2], Colton C. Katsarelis[3], Ching H. Su[4]
NASA Marshall Space Flight Center, Huntsville, AL 35812

Diana. Y. Andreev[5], Abram G. Culver[6]
Amentum Space Exploration Group, NASA Marshall Space Flight Center, Huntsville, AL 35812

The National Aeronautics and Space Administration (NASA) has been involved in the development and maturation of metal additive manufacturing (AM) for space applications since the late 2000s. AM has provided new design and manufacturing opportunities to reduce cost and schedule, consolidate parts, and optimize performance. Laser Powder Bed Fusion (L-PBF) is one of the most commonly used AM processes to fabricate components of complex shape requiring fine feature resolution. Due to exposure to high-pressure gaseous hydrogen, mechanical property degradation caused by hydrogen environment embrittlement (HEE) is a critical concern for many materials in liquid hydrogen propulsion systems. NASA has identified the need to develop and advance new materials in unique engine applications using liquid hydrogen as a propellant. One such material being developed at NASA Marshall Space Flight Center is L-PBF NASA HR-2 (Hydrogen Resistant-2), a high-strength Fe-Ni-based superalloy resistant to HEE. The chemistry of NASA HR-2 was formulated to meet requirements for key liquid rocket engine (LRE) components that operate in high-pressure hydrogen environments. Initial development and material characterization found that NASA HR-2 has excellent L-PBF printability, and its microstructure evolves well after heat treatment. This new alloy has undergone fundamental metallurgical evaluations, heat treatment studies, detailed microstructure characterization, and mechanical testing across a range of temperatures. Tensile testing was performed in a pressurized gaseous hydrogen (GH2) environment to assess its resistance to HEE. L-PBF NASA HR-2 has an average yield stress of 95 ksi, an ultimate tensile stress of 165 ksi, and a very high fracture elongation of 34 - 36% when tested in a high-pressure (5 ksi) hydrogen environment. The tensile property data confirms hydrogen has little influence on HR-2's ductility, strength, and fracture behavior. L-PBF NASA HR-2 is a promising option for many hydrogen-sensitive LRE components that require exceptional resistance to HEE. This paper will provide an overview of the L-PBF

[1] Principal Scientist, Materials Science and Metallurgy Branch
[2] Materials Engineer, Materials Science and Metallurgy Branch, AIAA Member
[3] Team Lead, Materials Science and Metallurgy Branch
[4] Principal Scientist, Materials Science and Metallurgy Branch
[5] Additive Manufacturing Engineer, Advanced Manufacturing Branch
[6] Intern, Materials Science and Metallurgy Branch

process development, material characterization, mechanical and thermophysical properties, and LRE hardware development for NASA HR-2.

I. Nomenclature

AM	=	Additive Manufacturing or Additively Manufactured
FCC	=	Face Centered Cubic
GHe	=	Gaseous Helium
GH_2	=	Gaseous Hydrogen
h or hrs	=	hours
HEE	=	Hydrogen Environment Embrittlement
HIP	=	Hot Isostatic Pressing
LP-DED	=	Laser Powder Directed Energy Deposition
L-PBF	=	Laser Powder Bed Fusion
LRE	=	Liquid Rocket Engine
Md	=	Average d-electron energy above the Fermi energy level
MSFC	=	Marshall Space Flight Center
PHACOMP	=	Phase Computation
UTS	=	Ultimate Tensile Strength
YS	=	Yield Strength

II. Introduction

The National Aeronautics and Space Administration (NASA) has been involved in the development and maturation of metal additive manufacturing (AM) for space applications since the late 2000s. AM has provided new design and manufacturing opportunities to reduce cost and schedule, consolidate parts, and optimize performance. Conventional production of high-performance metallic parts requires a costly and tedious manufacturing route that involves vacuum induction melting and vacuum arc melting, followed by hot or cold rolling or forging and machining to fabricate individual parts. In comparison, AM has demonstrated schedule savings of 2-10x over these traditional methods and cost reduction on the order of 50% or greater [1]. As such, AM has matured rapidly for use in propulsion systems with many components in both flight and developmental applications.

Mechanical property degradation of materials due to hydrogen environment embrittlement (HEE) from exposure to high-pressure gaseous hydrogen is a critical concern in liquid hydrogen propulsion systems [2, 3]. In light of this issue and the advantages of AM, NASA has identified the need to develop and advance new AM-optimized materials for use in the unique application of liquid rocket engines (LREs) using liquid hydrogen as a propellant [1,4-8].

One such material being developed at NASA Marshall Space Flight Center (MSFC) is L-PBF NASA HR-2 (Hydrogen Resistant-2). NASA HR-2 is a HEE resistant, Ni-Fe-based γ′-strengthened superalloy alloyed with Co, Cr, Mo, W, Ti, and Al for high strength and ductility. NASA HR-2 was derived from NASA HR-1 [2,7] to increase strength and enhance microstructure evolution from an as-built arc-shaped coarse structure to a fine equiaxed grain structure after post-processing heat treatment. The alloy development was approached by formulating a hydrogen-resistant γ-matrix that resembles NASA HR-1 along with increasing strength by promoting γ′ precipitation and solid-solution strengthening the γ matrix.

Laser Powder Bed Fusion (L-PBF) is an AM process in which parts are manufactured using a bed of powder and a laser as the energy source, and is favored for fabricating components of complex shape which require fine feature resolution. The precision of L-PBF and potential cost and schedule savings over the conventional manufacturing route provide a path for NASA HR-2 to become an affordable HEE resistant AM alloy for LRE applications.

Due to the excellent resistance to HEE, alloys A-286 and JBK-75 are being used in RS-25 engine for hydrogen sensitive components. However, both alloys have their limitations as they cannot be readily built using L-PBF. A-286 is very difficult to weld as it is highly susceptible to fusion zone hot cracking and heat-affected zone (HAZ) micro-fissuring [9]. JBK-75 is more weldable than A-286, but it was found to be susceptible to hot cracking during L-PBF [10]. In consideration of these problems, NASA HR-2 was specifically developed as a solution to fabricate hydrogen sensitive LRE components using the L-PBF technique. The development of L-PBF NASA HR-2 has advanced through process development using various L-PBF process parameters to assess their effect on defect formation, microstructure evolution, and process economics. L-PBF NASA HR-2 has undergone fundamental metallurgical

evaluations, heat treatment studies, detailed microstructure characterization, and mechanical testing across a range of temperatures.

To date, L-PBF NASA HR-2 alloy has demonstrated its excellent printability and potential for fabricating complex-shaped components for various LRE components that need HEE resistance to meet the requirements of LRE applications. Tensile testing was performed in 5 ksi gaseous hydrogen environment to assess its resistance to HEE. The tensile property data confirms hydrogen has little influence on its ductility, strength, and fracture behavior. L-PBF NASA HR-2 is a promising AM alloy for fabrication of many hydrogen-sensitive LRE components that require exceptional resistance to HEE. There were many observations and lessons learned from the development of L-PBF NASA HR-2. This paper details the development work completed for L-PBF NASA HR-2 including formulation, L-PBF build processes, heat treatment, microstructure characterization, and mechanical testing. The influence of process parameters on L-PBF printability and densification level was explored and compared. The latest advancement of the NASA HR-2 alloy in the L-PBF process maturity and LRE hardware development is also discussed. The development of L-PBF NASA HR-2 is funded under the grants provided by Jacobs TIPI program and the Liquid Engine Office at NASA Marshall Space Flight Center.

III. Alloy Chemistry Formulation

NASA HR-2 is a γ'strengthened Ni-Fe-based superalloy derived from NASA HR-1 [2,7] to increase strength and enhance microstructure evolution after post-processing heat treatment. The alloy development of L-PBF NASA HR-2 was approached by formulating a hydrogen-resistant γ-matrix that resembles NASA HR-1 along with increasing γ′ volume fraction and solid-solution strengthening the γ matrix. PHACOMP (PHAse COMPutation) [14-19] was used for L-PBF NASA HR-2 development to ensure stability of γ-matrix and prevent formation of deleterious η phase (Ni_3Ti) at grain boundaries. PHACOMP uses a parameter, *Md*, which is the average d-electron energy above the Fermi energy level of alloying elements in the alloy, to estimate the solid solubility of FCC (Face Centered Cubic) γ matrix. Overall, the alloy chemistry optimization for L-LBF NASA HR-2 follows the following criteria:

- *Md* level was kept close to that of NASA HR-1 to maintain stability of the γ (austenitic) matrix that is essential to mitigate η-phase (Ni_3Ti) formation at grain boundaries.
- Ni and Fe form the matrix of FCC γ phase, which acts as base or solvent for other elements in the alloy. The Ni:Fe ratio was increased slightly to depress *Md* level and improve solid solubility of the matrix γ phase.
- W is an important refractory element that provides persistent solid-solution strengthening at elevated temperatures. W was increased to 3.2% to reduce the stacking fault energy (SFE) of the alloy. Lowering the SFE has been shown to decrease the susceptibility to hydrogen embrittlement for several transition metal alloys [20]. Another benefit of increasing W content is that the degree of recrystallization after heat treatment increases due to reduction in the SFE [21].
- Similar to W, Mo is also a refractory element that provides persistent solid solution strengthening at elevated temperatures. Mo is also very effective in lowering the SFE for superalloys. Therefore, Mo content was increased up to 3.0% to enhance solid solution strengthening and microstructure evolution after post L-PBF heat treatment.
- Ti and Al are the primary strengthening elements in Ni-Fe-base superalloys as they combine with Ni to form the strengthening γ′ precipitate, $Ni_3(Ti,Al)$. Ti content was increased to 2.8% to obtain an optimal balance of strength and ductility.

PHACOMP can determine a critical *Md* value, above which microstructure instability occurs. For a Ni-Fe-based superalloy, the average value of *Md* can be calculated using Eq. (1).

$$Md = \sum_{i=1}^{n} X_i (Md)_i \quad (1)$$

Where:

Md = average *Md* parameter
X_i = the atomic fraction of the element i in the γ matrix
n = the number of elements in the alloy
$(Md)_i$ = the *Md* value for element *i*

The summation is taken over all the alloying elements, i=1,2…n. When *Md* increases beyond a critical value, the PHACOMP method assumes that the γ phase instability will occur and that a secondary phase will appear in a terminal

solid solution. In other words, the critical *Md* determines the solubility limit of the γ matrix. *Md* calculations were performed for NASA HR-2 to yield the *Md* values for two trial chemical compositions, hereafter referred to as "formulation I" and "formulation II".

The critical *Md* value that must be kept below to avoid η-phase formation for LP-DED NASA HR-1 is around 0.9134 [7]. Therefore, the *Md* values for L-PBF NASA HR-2 was kept very close to 0.9134 to improve the γ matrix stability and mitigate precipitation of η-phase. An important consideration for the L-PBF NASA HR-2 composition formulation is its excellent HEE resistance should not be altered. Based on the above approaches, the chemical composition for L-PBF NASA HR-2 was formulated as shown in Table 1. Fig. 1 compares the *Md* values for the alloys listed in Table 1. Maintaining the *Md* value very close to that of LP-DED NASA HR-1 is expected to mitigate precipitation of the undesirable grain boundary η-phase and enhance HEE resistance. In addition, higher W content in NASA HR-2 formulation II (than in NASA HR-1) can retard the metastable γ′ to stable η-phase transformation during aging treatment by decreasing the diffusivity of Ti atoms or by increasing the formation of stacking faults [2].

Table 1. Nominal chemical composition (wt%) for L-PBF NASA HR-2. The *Md* level of LP-DED NASA HR-1 was used as the critical threshold *Md* value for L-PBF NASA HR-2.

Alloy	Fe	Ni	Cr	Mo	V	W	Co	Ti	Al	***Md***
L-PBF NASA HR-2 Formulation I (F1)	30.85	42.00	15.00	1.80	0.10	3.20	4.00	2.80	0.25	**0.9135**
L-PBF NASA HR-2 Formulation II (F2)	30.00	41.50	15.50	3.00	-	3.20	4.00	2.80	0.25	**0.9206**
LP-DED NASA HR-1	41.20	34.00	14.60	1.80	0.30	1.60	3.80	2.40	0.25	**0.9134**

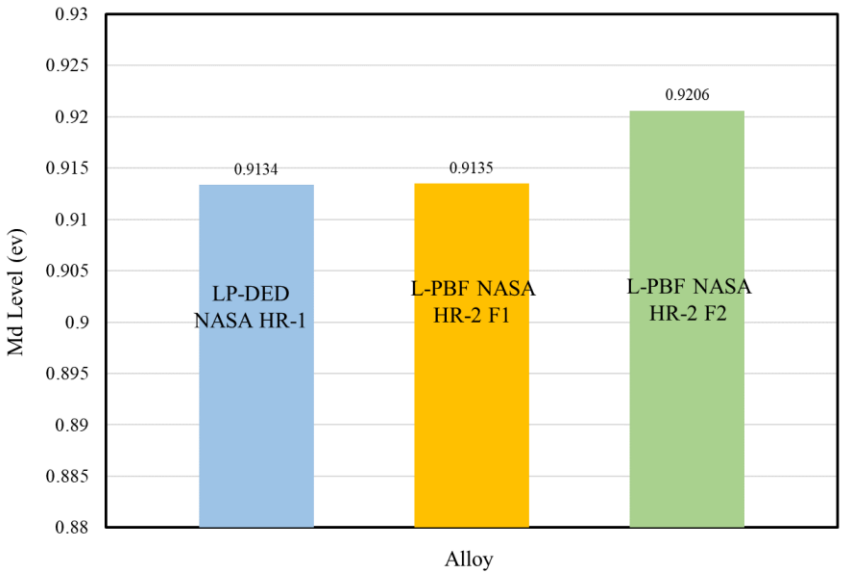


Fig. 1 *Md* comparison for L-PBF NASA-HR-2 and LP-DED NASA HR-1.

IV. Experimental Procedures and Methods

A. Material and L-PBF Process

The material used in this study was pre-alloyed NASA HR-2 powder supplied by PAC (Powder Alloy Corporation), located in Loveland, Ohio. The analyzed chemical composition of NASA HR-2 powder and its specification is provided in Table 2. The specified powder size distribution is between 10 and 45 μm (+35 mesh/1250 mesh). The morphology of powders was observed using a Hitachi scanning electron microscopy (SEM) with an

accelerating voltage of 15 kV. The SEM images showing the typical NASA HR-2 powder morphology for L-PBF process are presented in Fig. 2. NASA HR-2 powder is mostly spherical shape with occasional satellites and agglomerations. These satellites are believed to form when the faster-solidified finer particles adhere to the molten or semi-solid surface of the coarser particles due to the in-flight collisions among the particles during the gas atomization process [19].

Table 2. Analyzed chemical composition (wt%) of NASA HR-2 powder and its specification.

Wt.%	NASA HR-2 Formulation I				NASA HR-2 Formulation II			
Element	**Analyzed**	**Nominal**	**Min**	**Max**	**Analyzed**	**Nominal**	**Min**	**Max**
Fe	31.18	30.85	30.4	31.3	30.99	30	29.6	30.4
Ni	41.9	BAL			BAL	41.5		
Cr	15.19	15	14.7	15.3	15.65	15.5	15.2	15.8
Co	3.95	4	3.8	4.2	3.8	4	3.8	4.2
Mo	1.84	1.8	1.3	2	2.98	3	2.8	3.2
W	2.96	3.2	3	3.4	3.14	3.25	3	3.4
Ti	2.59	2.8	2.7	2.9	2.55	2.8	2.7	2.9
V	0.1	0.1	0.05	0.15				
Al	0.26	0.25	0.2	0.3	0.24	0.25	0.2	0.3
S	<0.01			0.005	<0.01			0.005
P	<001			0.005	<001			0.005
C	0.01			0.03	0.01			0.03
Si	0.02			0.05	0.02			0.05
B	<0.05			0.005	<0.05			0.005
Mn	0.03			0.05	0.03			0.05
H	3 ppm			<50 ppm	3 ppm			<50 ppm
O	240 ppm			<300 ppm	610 ppm			<300 ppm
N	97 ppm			<200 ppm	78 ppm			<200 ppm

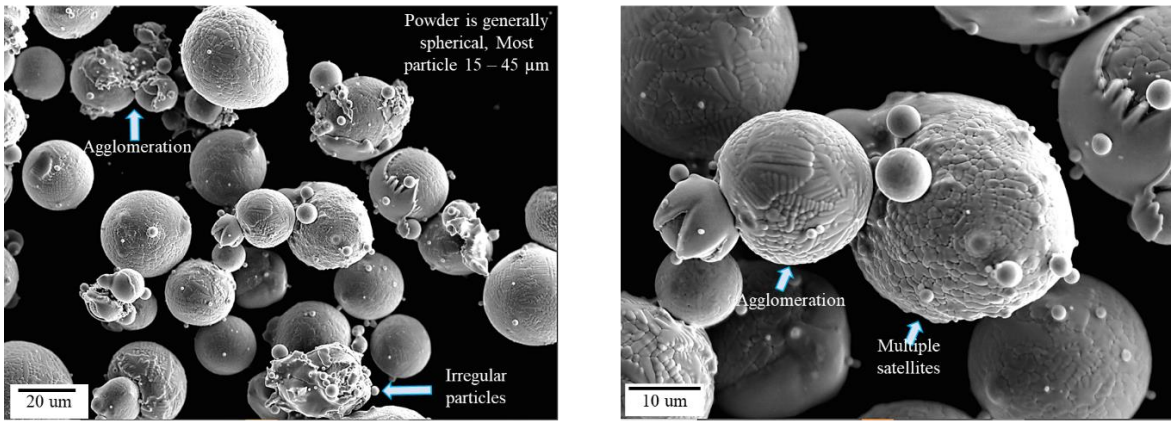


Fig. 2 SEM images showing NASA HR-2 powder particle morphology (formulation II).

The manufacturing of L-PBF NASA HR-2 samples was performed in an EOS M100 system at NASA MSFC. A screen size of 63 µm was used to filter out large powder particles. The scanning strategy includes remelting of each layer, where the layer is scanned with a rotation of 67° between the scanning vectors. It has been reported that a 67˚ rotation in the scanning direction results in different heat flow direction in successive layers. As a result, grain orientation is more random without a particular predominant crystallographic texture in the microstructure. The reduced anisotropy in microstructure can be attributed to the disruptive grain growth caused by the rotating laser scanning path in the sample [20]. It must be noted that the M100 system built samples with a restriction angle of 30 ° to avoid laser scanning parallel to the Ar gas flow direction (y-direction). The 67° rotation angle was skipped and

rotated by additional 67° when the scanning direction was within a range of ± 30° from the y-direction [21]. In addition, the laser scanned area is partitioned into 5 mm width stripes with 0.1 mm overlap so that the laser tracks are not appreciably large. In L-PBF, laser power, scanning speed, hatch spacing, and layer thickness are the typical process parameters. Parameter development was performed to determine the optimum parameter that can produce defect-free and dense parts. An illustration of parameter development sample fabrication via L-PBF process is shown in Fig. 3. The sample distribution inside the M100 machine for parameter development samples, round bar tensile and metallographic samples is shown in Fig. 4. The tensile samples were deposited to a length of 2.5 inches and 0.375 inches in diameter.

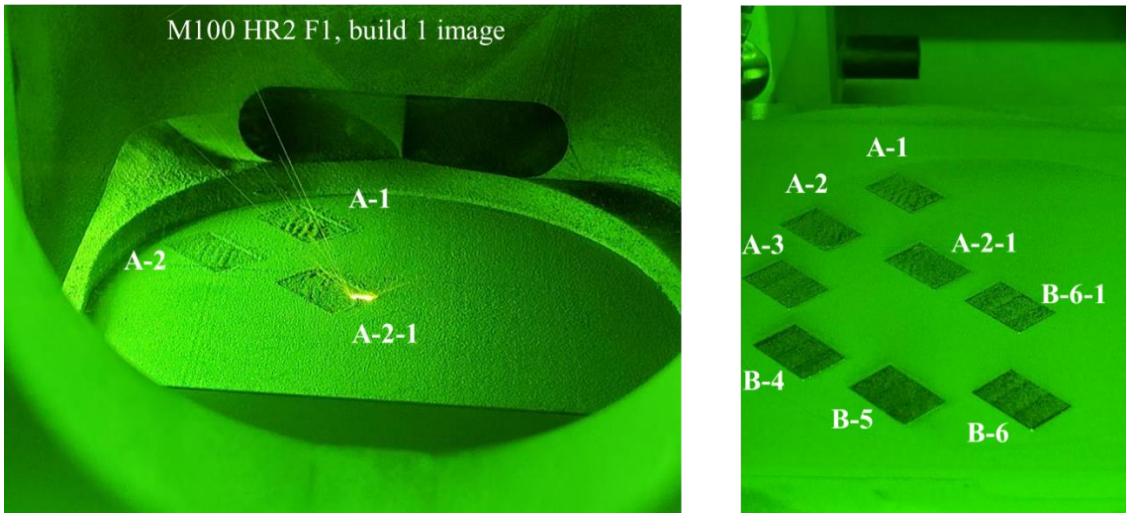


Fig. 3 An illustration of NASA HR-2 parameter development sample fabrication via L-PBF.

B. Heat Treatment

After L-PBF deposition, the as-built samples require post-processing heat treatment to attain the desirable microstructure and materials properties. The heat treatment steps include a stress relief, homogenization, solution anneal, and aging treatment. The as-built samples received stress-relief treatment in vacuum at 1950 °F/1.5h with a slow furnace cool. After stress relief, the samples were subjected to a HIP cycle at 2125 °F/15ksi/3h. Then, the samples were solution annealed at 1950 °F/1h in vacuum with an argon quench. Finally, a 2-step aging cycle was perforemed at 1275 °F/16h + 1150 °F/16h (total 32 hours) in a vacuum furnace to complete the heat treatment process.

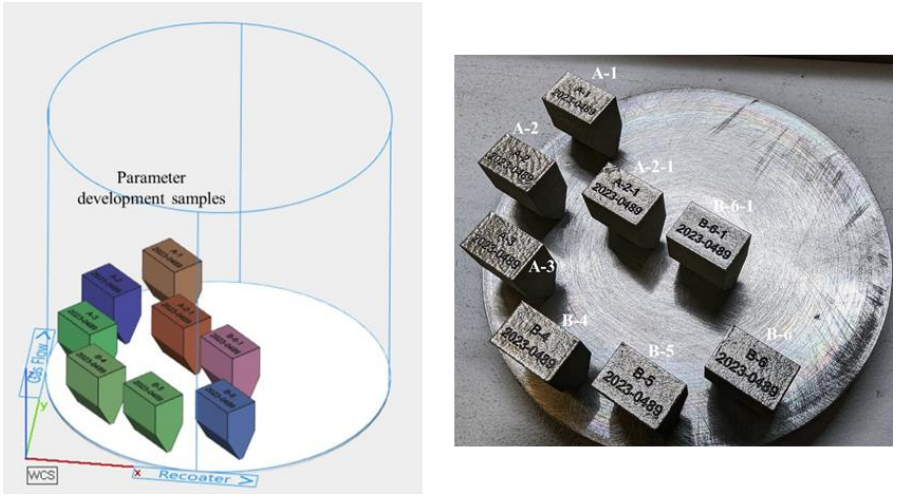
C. Metallography and SEM analysis

Selected L-PBF NASA HR-2 specimens were metallurgically characterized after heat treatment and mechanical testing. Specimens were sectioned, mounted, ground, and polished using standard metallographic procedures with a series of 220-2,000 grit paper and 3 μm diamond suspension on 0.05 μm alumina pads. Chemical etching was conducted with waterless Kaling's reagent immersed for 5–10 seconds. Fresh acedic glyceregia exchant was used to reveal the melt pool structrue of as-built samples. Microstructures of as-deposited and heat treated L-PBF NASA HR-2 were examined via optical (Leica DMi8 A) and scanning electron microscopy (SEM) (Hitachi S-3700N). High resolution optical montage images were taken to document the microstructure for the entire sample.

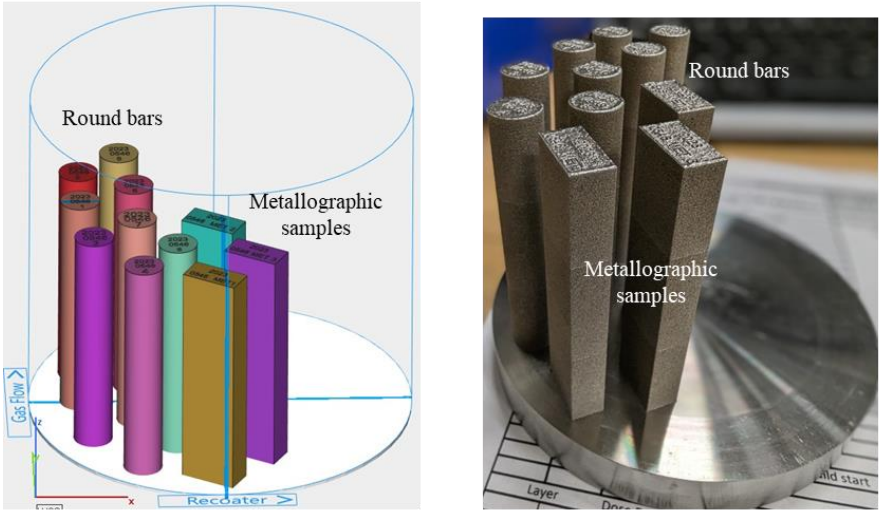
D. Mechanical Testing

Tensile testing was performed in ambient air with a strain rate of 0.5 in/in/min at three different temperatures, -320 °F, room temperature, and 1200 °F. Elevated temperature tensile testing was conducted using a Mayes elevated temperature extensometer (Model: R3/8 Block 2) on an Instron load frame equipped with a 250 kN load cell according to guidelines established in ASTM E21 (Standard Test Methods for Elevated Temperature Tension Tests of Metallic Materials). Room temperature testing was conducted using an Instron 5582 load frame equipped with a 100 kN load cell and an Instron model 2620 extensometer according to guidelines established in ASTM E8 (Standard Test Methods for Tension Testing of Metallic Materials). Smooth tensile testing performed at room temperature in ambient air was used as the baseline tensile properties without the influence of hydrogen. Tensile testing was also performed in a 5 ksi

high pressure gaseous hydrogen environment (GH_2) at the NASA-MSFC Hydrogen Test Facility (HTF) in Test Cell 23 (TC-23). The smooth tensile sample had a uniform gage, 0.188 inch in diameter by 0.75 inch in length. The specified surface finish (Ra, value of arithmetic mean surface roughness) for the gauge section was 32 μin or better. Shape and dimension of the smooth tensile specimen used for testing at ambient temperature in 5 ksi gaseous hydrogen environment is shown in Fig. 5. Final machining of the gauge section was performed by low stress grinding per ASTM standard G142. Smooth tensile testing in hydrogen was performed at a pre-yield strain rate of of 0.005 in/in/min to failure. Fracture elongation was obtained based on the change in the total length of the specimen gauge (0.75 inch gauge length) before and after the test. HEE susceptibility was evaluated by the relative fracture elongation, which is a ratio of fracture elongation in high pressure gaseous hydrogen (GH_2) to that in ambient air.



(a)



(b)

Fig. 4 Sample distribution inside the M100 machine for (a) parameter development samples, (b) round bar tensile and metallographic samples. The tensile samples were deposited to a length of 2.5 inches and 0.375 inches in diameter.

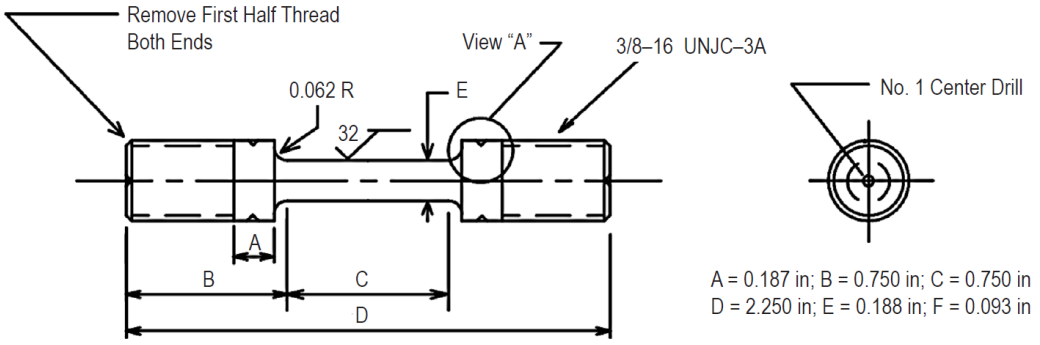


Fig. 5 Geometry and dimensions of the smooth tensile specimen used for testing in a 5 ksi gaseous hydrogen environment at ambient temperature. All dimensions are in inches. The specified surface finish (Ra) on the gauge surface is 32 µin or better. Low stress grinding (LSG) was used to produce specimens with the specified surface finish.

V. Results and Discussion

A. L-PBF Parameter Development

During the L-PBF parameter development stage, six different sets of process parameters were employed to fabricate samples. As shown in Table 3, specimens were fabricated by varying laser power, scan speed, and hatch spacing, while keeping the layer thickness constant at 0.02 mm. The laser power varies from 107 to 170 W, the scan speed and hatch spacing change from 827–1500 mm/s, and 0.055–0.07 mm, respectively. The layer thickness is kept at 0.02 mm for all parameters. Parameter A-1 has the highest volumetric energy density and A-3 has the lowest volumetric energy density. Relative processing time, which denotes the time (seconds) needed to print a 2500 mm^2 area, is also given in Table 3. An illustration of L-PBF NASA HR-2 parameter development samples on the building plate is shown in Fig. 4(a). Developing a process parameter that can improve parts quality and maintain an acceptable processing time is a crucial objective for L-PBF parameter development.

Table 3. L-PBF parameters for the fabrication of parameter development samples. Relative processing time denotes the time (seconds) needed to print a 2500 mm^2 area.

Parameter	Power (W)	Scan Speed (mm/s)	Hatch Spacing (mm)	Layer Thickness (mm)	Volumetric Energy Density (J/mm^3)	Relative Processing Time (s)
A-1	170	1500	0.055	0.02	103.03	30.30
A-2	170	1500	0.060	0.02	94.44	27.78
A-3	170	1500	0.065	0.02	87.18	25.64
B-4	170	1300	0.070	0.02	93.41	27.47
B-5	140	1200	0.060	0.02	97.22	34.72
B-6	107	827	0.070	0.02	92.42	43.19

B. Porosity Analysis

Porosity is a common defect in metal AM parts and can negatively affect mechanical properties. A good build quality should have very low fraction of porosity in the microstructure. Therefore, the influence of process parameters on the void content was explored and compared. Porosity was measured on the parameter development samples that were built with six (6) different L-PBF parameters. Each polished sample was observed via optical microscopy (Leica DMi8 A) to analyze the void content. The micrographs were then processed using ImageJ processing software to convert pores into black pixels using a thresholding tool. The percentage of black pixels versus the total number of

pixels for each micrograph was determined. Porosity was then calculated by averaging the percentages of black pixels in the micrographs for each parameter per ASTM E2109-01 standard (2014).

The porosity area fraction analysis results and representative optical micrographs of the L-PBF NASA HR-2 (formulation II) samples in the as-polished condition are shown in Fig. 6. Porosity is very low and varies slightly with the build parameters from 0.01% in sample B-4 to 0.043% in sample B-6. There are no signs of defects, such as lack of fusion and micro-cracks, in the samples. Fig. 7 compares the measured porosity as a function of L-PBF process parameter for both formulations. It is significant to note that L-PBF NASA HR-2 can achieve very low porosity in the as-built condition. As shown in Fig. 11, formulation II can achieve lower porosity than formulation I, but the trend of L-PBF parameter effect on porosity is similar for both formulations. Judging from the porosity level and relative processing time, B-4 apereas to be the most promising parameter and was used to fabricate tensile and metallographic samples.

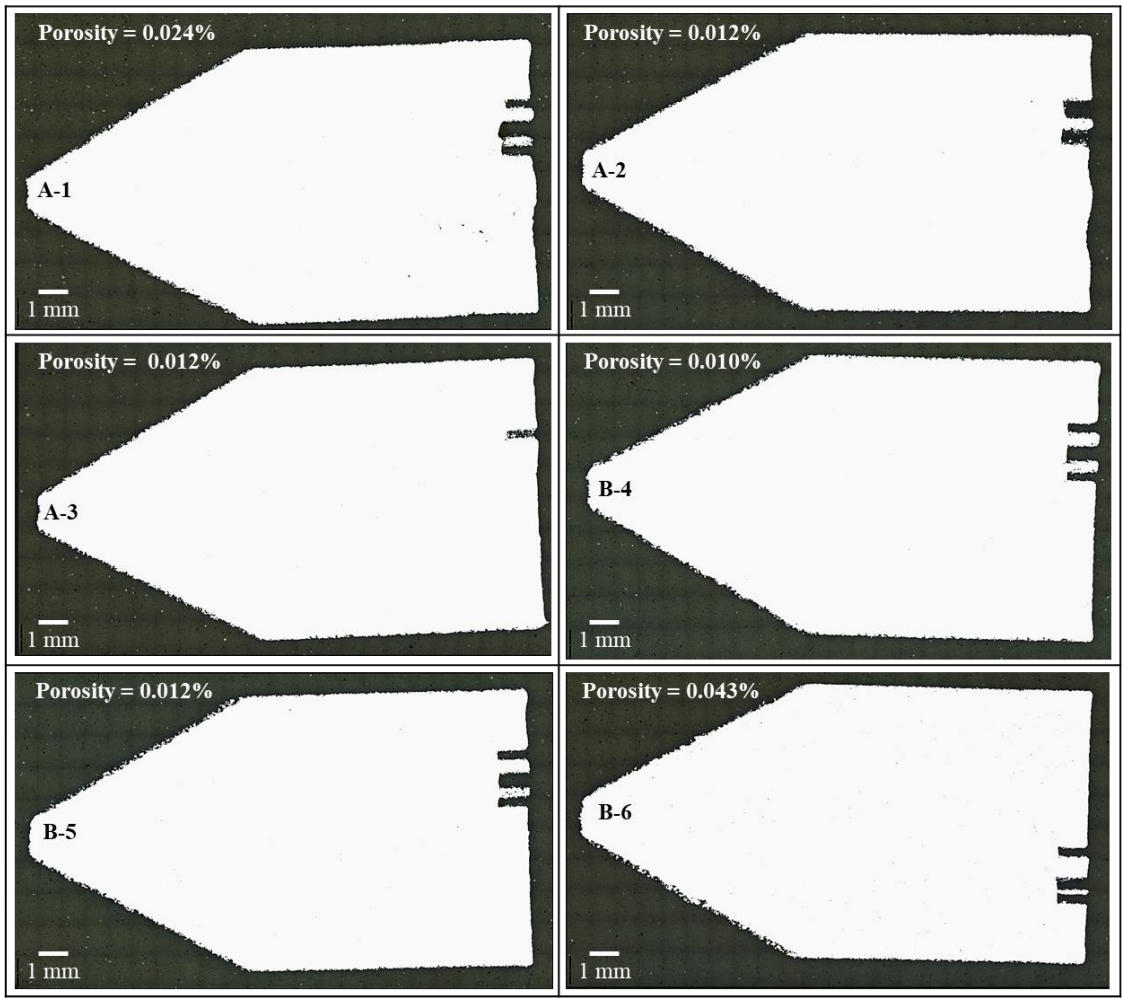


Fig. 6 Optical micrographs showing L-PBF NASA HR-2 samples (formulation II) in the as-polished condition. Porosity is very low and varies slightly with the build parameters.

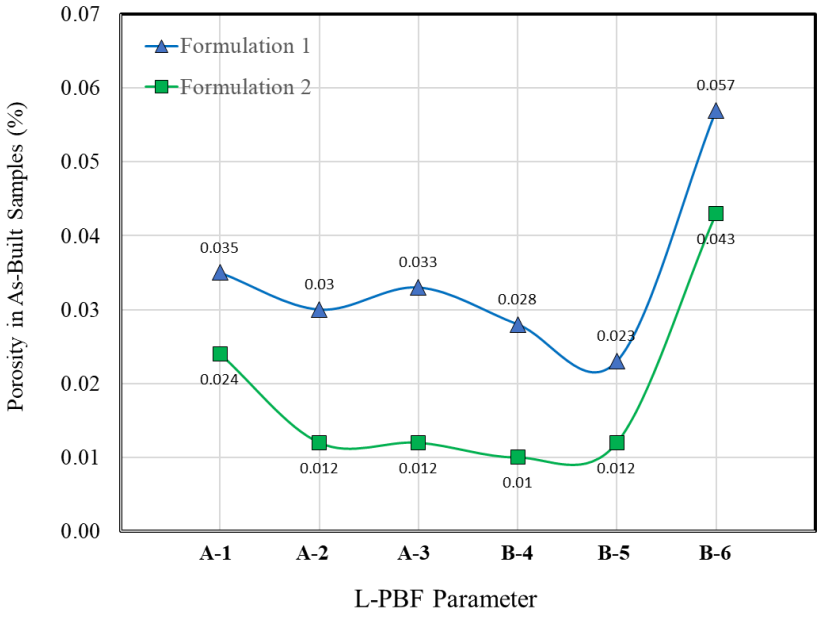


Fig. 7 Measured porosity vs. process parameter for L-PBF NASA HR-2.

Although B-6 can achieve better surface quality, its slow scan speed will increase the total build time significantly. All in all, an optimum balance of surface quality and build time can be obtained from parameter B-4 (as shown in Table 3 and Fig. 6) that have the optimal balance of laser power, scanning speed (total build time), and hatch spacing.

C. As-Deposited Microstructure

The melt pool microstructure characteristics in terms of the size and shape of the melt pools and the distribution of micro-pores were investigated to determine how L-PBF parameters influence the as-deposited microstructure. In the as-built state, the L-PBF manufactured NASA HR-2 microstructure exhibits arc-shaped structure due to the layer-by-layer building process. The as-built microstructure in the XZ cross section (parallel to the build direction) showing overlapping melt pools and the top layer is shown in Fig. 8. It can be clearly seen from the top layers that there are appreciable variation in the melt pool shape and depth due to the change in the build parameters. Melt pool depth for all samples varies from 83 - 107 µm. Sample A-1 clearly exhibits a higher degree of melt pool overlap than the others as it has the smallest hatch spacing (0.055mm). As can be seen in Fig. 8, the depth of melt pool is greater in sample B-6 than in the others, which likely results from the reduction in scan speed from 1500 mm/s to 827 mm/s. Some spherical pores are present, but they are very fine and randomly distributed throughout the samples. Most pores are smaller than 2 µm in diameter. Studies indicate the formation of fine spherical pores can be attributed to interlayer melting or argon gas being trapped within the material [22, 23].

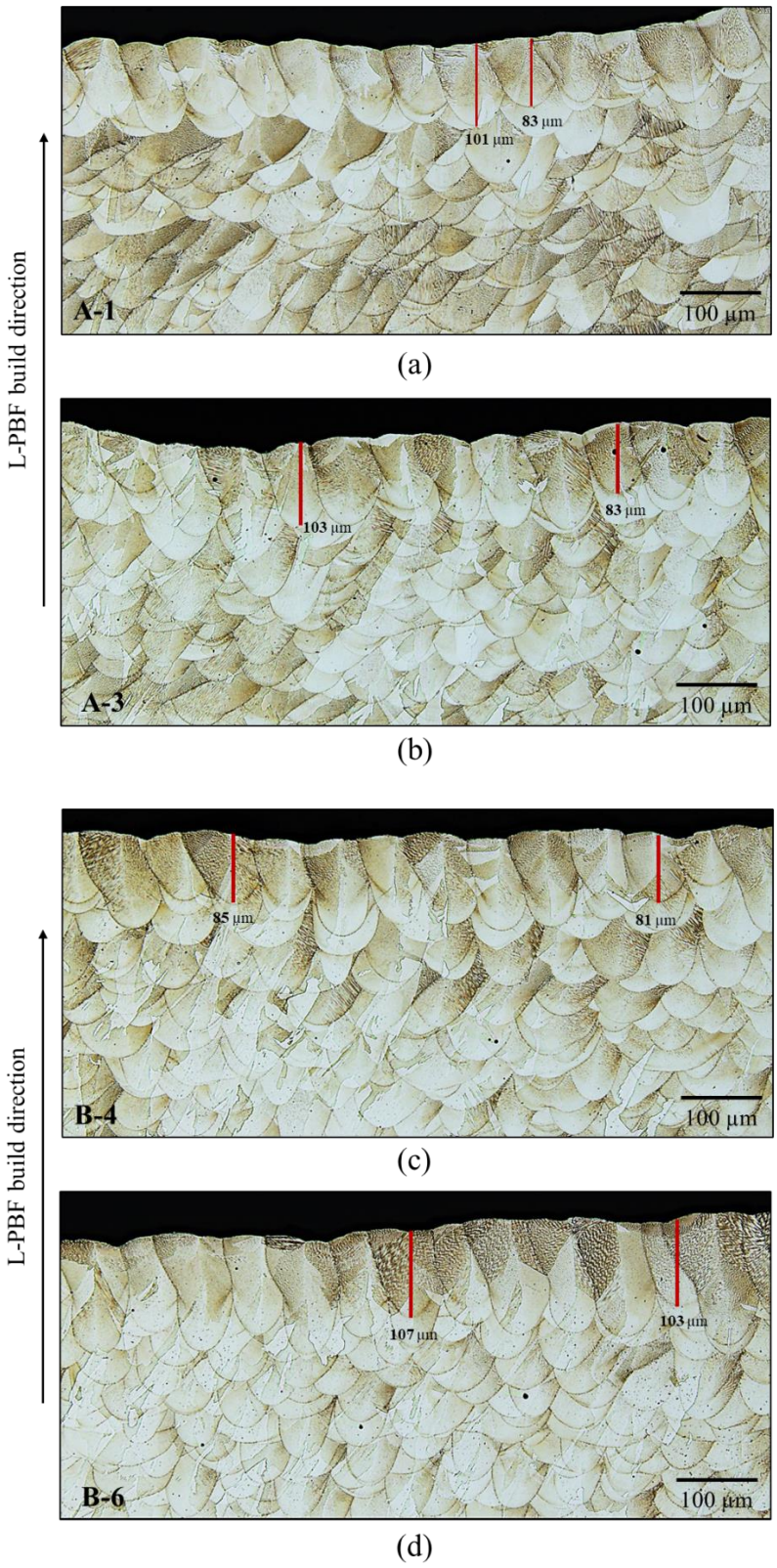


Fig. 8 The as-built microstructure in the XZ cross section (parallel to the build direction) showing overlapping melt pools and the top layer for samples (a) A-1, (b) A-3, (c) B-4, and (d) B-6.

Fig. 9 shows the as-built microstructure in the XY cross section. The cross hatches that rotate between two successive layers can be discerned as there is a diagonal pattern across the micrograph. The scanning strategy includes remelting of each layer, where the layer is scanned with an angular rotation of 67° between the scanning vectors. The 67° rotation was used as it was believed that at this value the scan vector direction would not repeat (to within 10° error) for the maximum number of layers [24]. With this scanning strategy, it was reported that a significant reduction in warping, defects, and anisotropy can be achieved in addition to the improvised surface roughness [25]. This type of hatch pattern is widely adopted by the additive manufacturing industry [26]. The 3D microscopy image showing the as-built microstructure (built with B-4 parameter) in three different orientations (XY, XZ, and YZ planes) is presented in Fig. 10. Elongated columnar grains can be seen extending through several melt pools on the XZ and YZ planes.

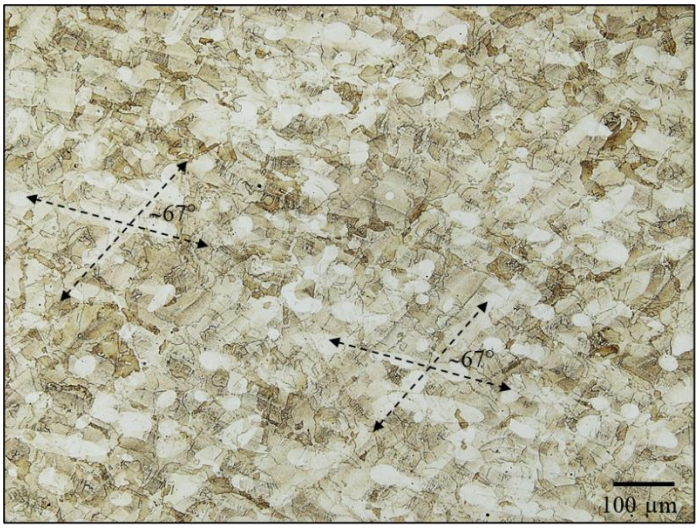


Fig 9. The as-built microstructure in the XY cross section clearly reveals the scanning strategy with an angular rotation of approximately 67° between layers (built with B-4 parameter).

D. Post-Processing Heat Treatment

During L-PBF process, the material is deposited layer by layer by a high-power laser beam and is subjected to a complex thermal cycle that includes rapid heating above the melting temperature and rapid cooling and solidification of the molten material. Thus, the L-PBF material always has high residual stress, heterogeneous microstructures, porosity, non-uniform chemical composition and phase distribution. Thermal post-processing (heat treatment) must be used to relieve residual stress, minimize the void content, and achieve the desired microstructure evolution and mechanical properties. The heat treatment for L-PBF NASA HR-2 consists of stress relief, hot isostatic pressure treatment (HIP), solution anneal, and aging treatment. A stress relief cycle was performed as the first step prior to removing the parts from the build plate. After stress relief, the samples were subjected to a HIP cycle in an argon atmosphere to reduce porosity in as-fabricated parts. Then, the samples were solution annealed in vacuum with an argon quench to minimize η-phase (Ni_3Ti) precipitation. Solution annealing is often referred to as solution treatment or solutioning, is a specific annealing process that dissolves existing precipitates back into the solid solution. Finally, the samples were heat treated with a 2-step aging cycle in a vacuum furnace to precipitate and grow the strengthening γ′ precipitate. The optimized heat treatment process for L-PBF NASA HR-2 is shown below:

- Stress relief at 1950 °F for 1.5 hours in vacuum, followed by slow furnace cool,
- HIP at 2125 °F under a pressure of 15 ksi for 3 hours in an argon atmosphere,
- Solution annealing at 1950 °F for 1 hour in vacuum, followed by an argon quench,
- 2-step aging at 1275 °F for 16 hours and 1150 °F for 16 hours in vacuum.

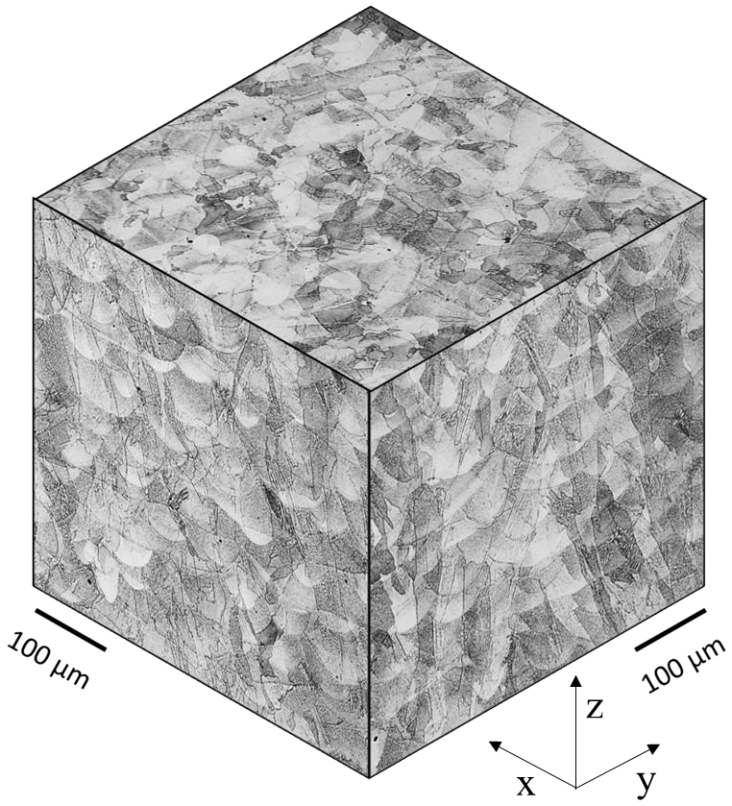


Fig. 10. Quasi-3D microscopy showing the as-built microstructure (B-4 parameters) in three different orientations, XY, XZ, and YZ. Elongated columnar grains can be seen extending through several melt pools on the XZ and YZ planes.

E. Microstructure Evolution after Stress Relief and HIP

Fig. 11 presents the SEM images showing microstructure evolution after heat treatment for formulation II samples built with B-4 parameter. Stress relief treatment activates recovery process by atomic diffusion from regions of higher stress to regions of lower stress, resulting in the relief of internal strain energy [27]. An effective stress relief can mitigate residual stresses and minimize the potential distortions. For L-PBF NASA HR-2, recovery and partial recrystallization occurred during stress relief at 1950 °F for 1.5h as shown in Fig. 11(b). After stress relief, the samples are subjected to a HIP treatment at 2125 °F to close internal pores, reduce elemental segregation, and promote recrystallization. As shown in Fig. 11(c), a complete transformation in microstructure occurs after HIP at 2125 °F and 15 ksi for 3 hours. The as-built microstructure evolves well into fine equiaxed grain structure after HIP treatment. A high degree of recrystallization is desirable for L-PBF NASA HR-2 to promote the formation of fine equiaxed grain structure from the as-built columnar dendritic microstructure. After HIP, solution anneal and aging processes are performed sequentially to precipitate and grow the strengthening γ′ precipitate (Ni_3(Ti,Al)). The primary objective of solution treatment is to dissolve the remnant η phase that may have formed during the slow cooling process after HIP. After completion of the solution anneal cycle in vacuum, the material is rapidly cooled by argon quench to maintain η-phase free solid solution. The solution annealing and aging cycles after HIP does not lead to further recrystallization and reduction in grain size as shown in Fig. 11(c) and (d).

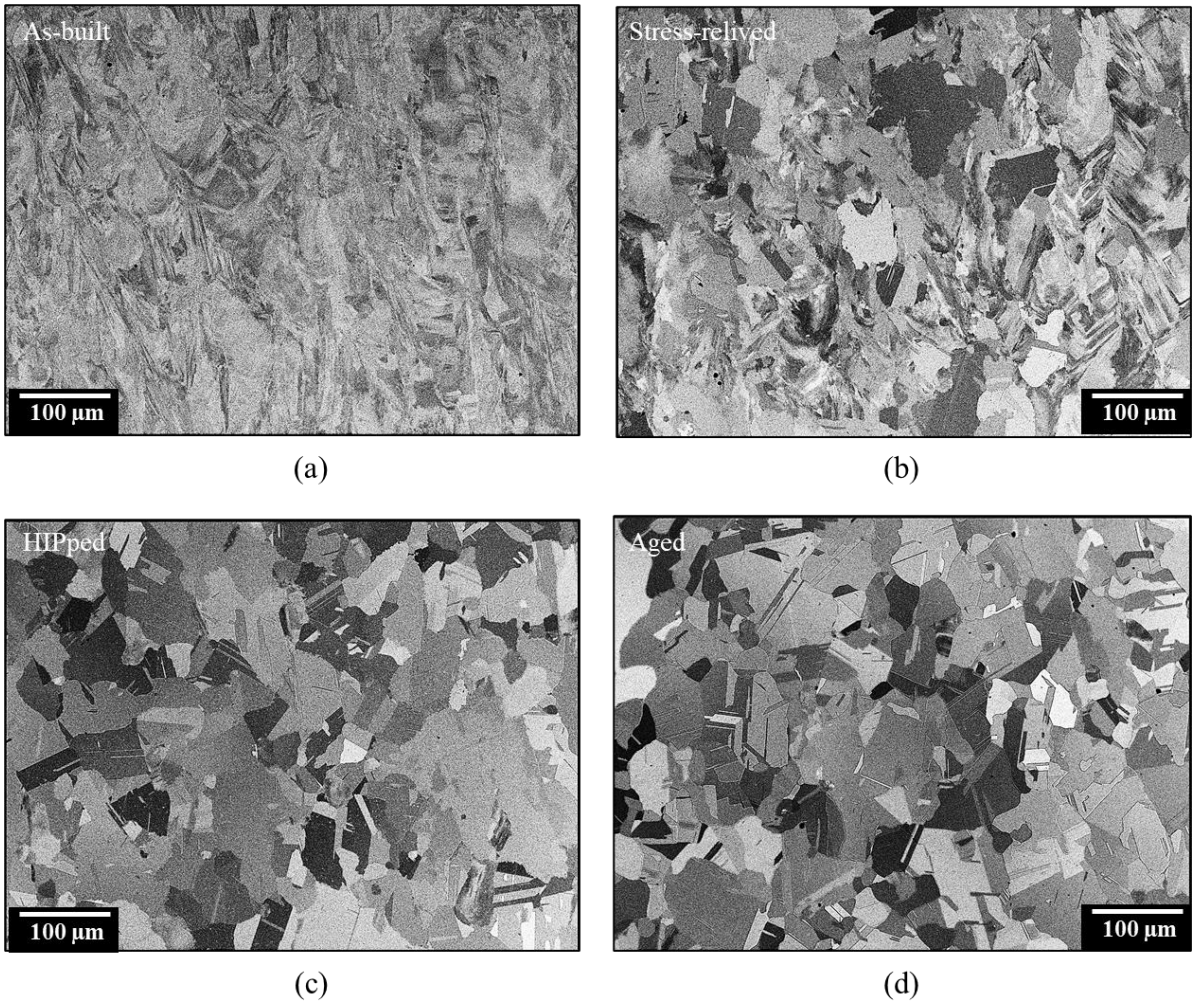


Fig. 11 SEM images showing microstructure evolution on the XZ plane in (a) as-built condition, and after (b) stress relief, (c) HIP, and (d) solution anneal and age. The sample was built with B-4 parameter. Solution annealing after HIP does not lead to further recrystallization and reduction in grain size.

Fig. 12 shows the influence of L-PBF process parameters on microstructure evolution (on the XZ plane) after HIP. It is obvious that a high degree of recrystallization had taken place after HIP at 2125 °F and 15 ksi for 3hrs. The driving force for recrystallization is the residual stress from the additive manufacturing process [28-31]. During the L-PBF process, the rapid heating and cooling cycles along with the volume change of the molten metal upon solidification result in buildup of residual stress in the parts. It is apparent that the residual stress in the as-built condition is quite high that a high degree of recrystallization occurred after heat treatment. Overall, the grain size of L-PBF NASA HR-2 after HIP is quite small and many grains in the material are smaller than 50 µm in diameter. Grain boundaries are very clean and free of the brittle η-phase (Ni_3Ti), which is critical in achieving a high resistance to hydrogen environment embrittlement. As can be seen in Fig. 12, it is apparent that B-4 exhibits a higher degree of recrystallization and smaller gain size than the others.

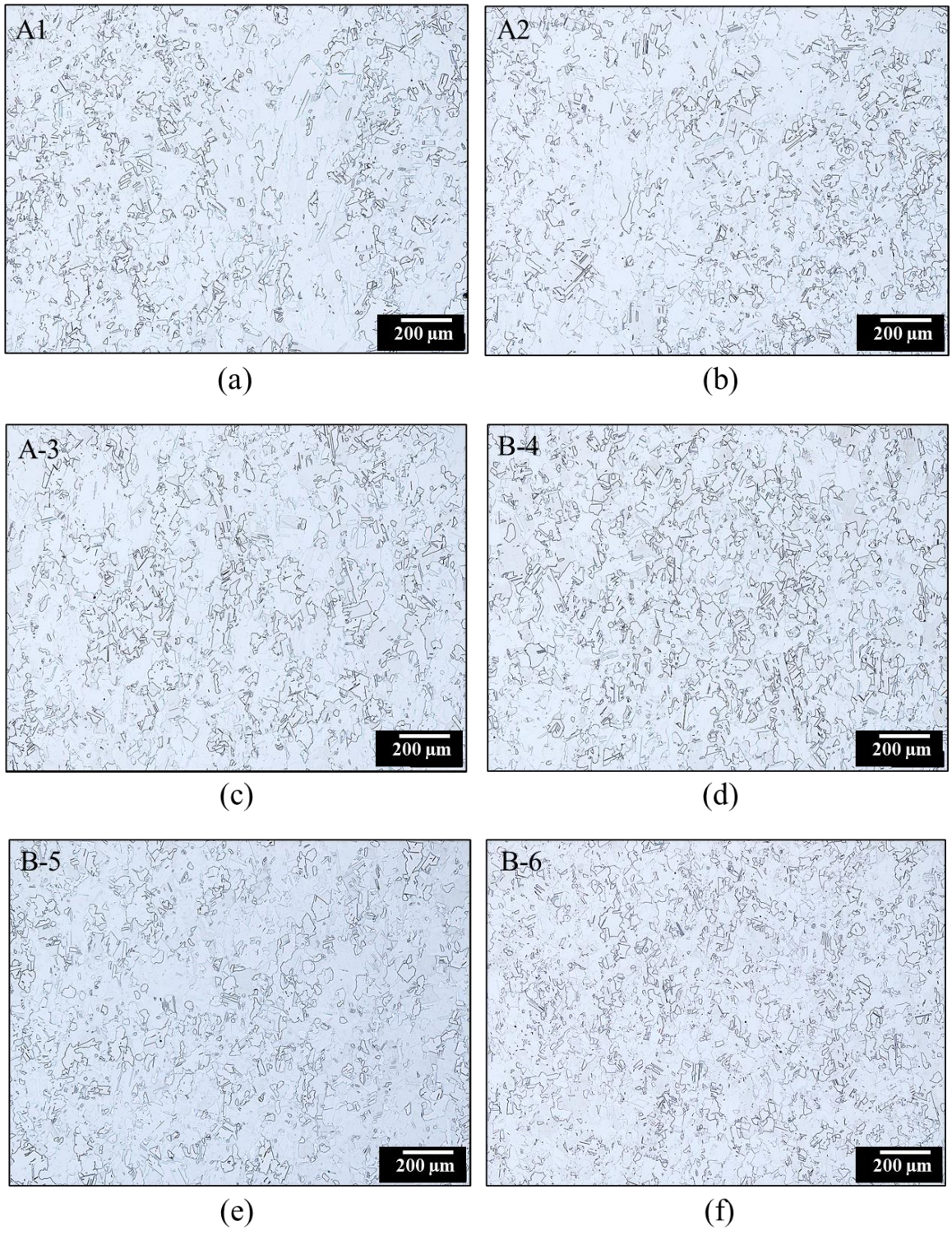


Fig. 12 Varying degree of recrystallization occurred after the material was HIPed at 2125 °F/15ksi/3h. The samples were built with (a) A-1, (b) A-2, (c) A-3, (d) B-4, (e) B-5, and (f) B-6 parameters. The viewing surface is the XZ plane. Sample B-4 exhibits a higher degree of recrystallization and smaller gain size than the others.

In general, a high degree of recrystallization is desirable as it can reduce anisotropy in mechanical properties. It has been reported that the tensile properties of L-PBF IN738LC strongly depend on whether recrystallization was

completed [32]. A low degree of recrystallization will result in anisotropy that is undesirable may significantly affect the mechanical properties [28]. Mechanical anisotropy was observed in additively manufactured Hastelloy X with a low degree of recrystallization [20]. The un-recrystallized columnar grains reduce the total number of grain boundaries along the build direction (BD), leading to higher fracture elongation and lower UTS when loaded along the BD. In contrast, the grain size in the transverse direction (TD) was approximately three times smaller than that in the BD and therefore results in a higher UTS and lower fracture elongation [20]. Anisotropy in tensile behavior can be attributed to low degree of recrystallization that changes grain orientation, shape, and crystallographic texture [33]. The selection on an optimum L-PBF parameter to fabricate tensile samples is evaluated based on various quality factors such as porosity, microstructure (evolution), and relative processing time. After a thorough evaluation on the quality factors, B-4 appears to be the most promising parameter and was selected to fabricate tensile samples. The grain structure in the XY and YZ orientations are also very fine and equiaxed throughout as shown in Fig. 13. 3D images showing microstructure evolution of B-4 samples before and after post-processing heat treatment are shown in Fig. 14 (for formulation II).

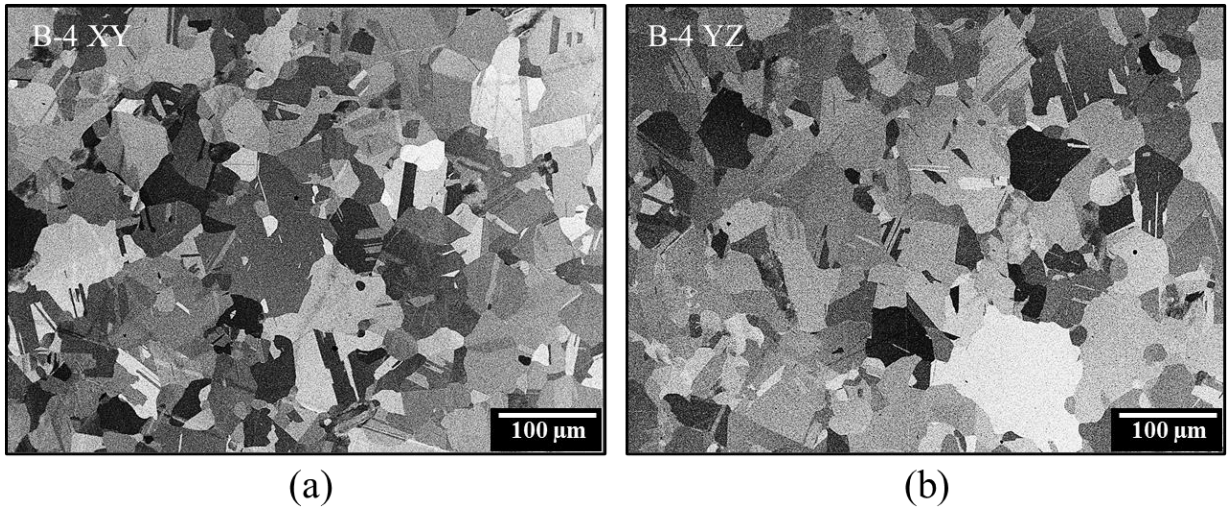


Fig. 13. SEM images showing recrystallized grain structurer in (a) XY and (b) YZ orientations for sample built with B-4 parameter.

F. Temperature-Dependent Tensile Properties in Ambient Air

Temperature–dependent tensile properties of L-PBF NASA HR-2 were investigated using fully heat-treated samples. L-PBF NASA HR-2 round bar was machined into a cylindrical shaped tensile specimen along the build direction with a gauge length of 0.75 inch and 0.188 inch in diameter. Table 4 summarizes the tensile properties of L-PBF NASA HR-2 as a function of testing temperature at –320°F, room temperature, and 1200 °F. It can be seen from Table 4 that both YS and UTS decrease with an increase in the test temperature from room temperature to 1200 °F. UTS/YS ratio also decrease as the test temperature increases up to 1200 °F. UTS/YS ratio, which correlates well with strain hardening exponent, can be used to estimate static strain hardening capability [34]. Tensile fracture elongation is very high around 39 - 42% at –320 °F and decreases slightly to 34 - 38% at room temperature. A significant reduction in ductility was noted when the testing temperature increased to 1200 °F, which hints a change in the deformation mechanism.

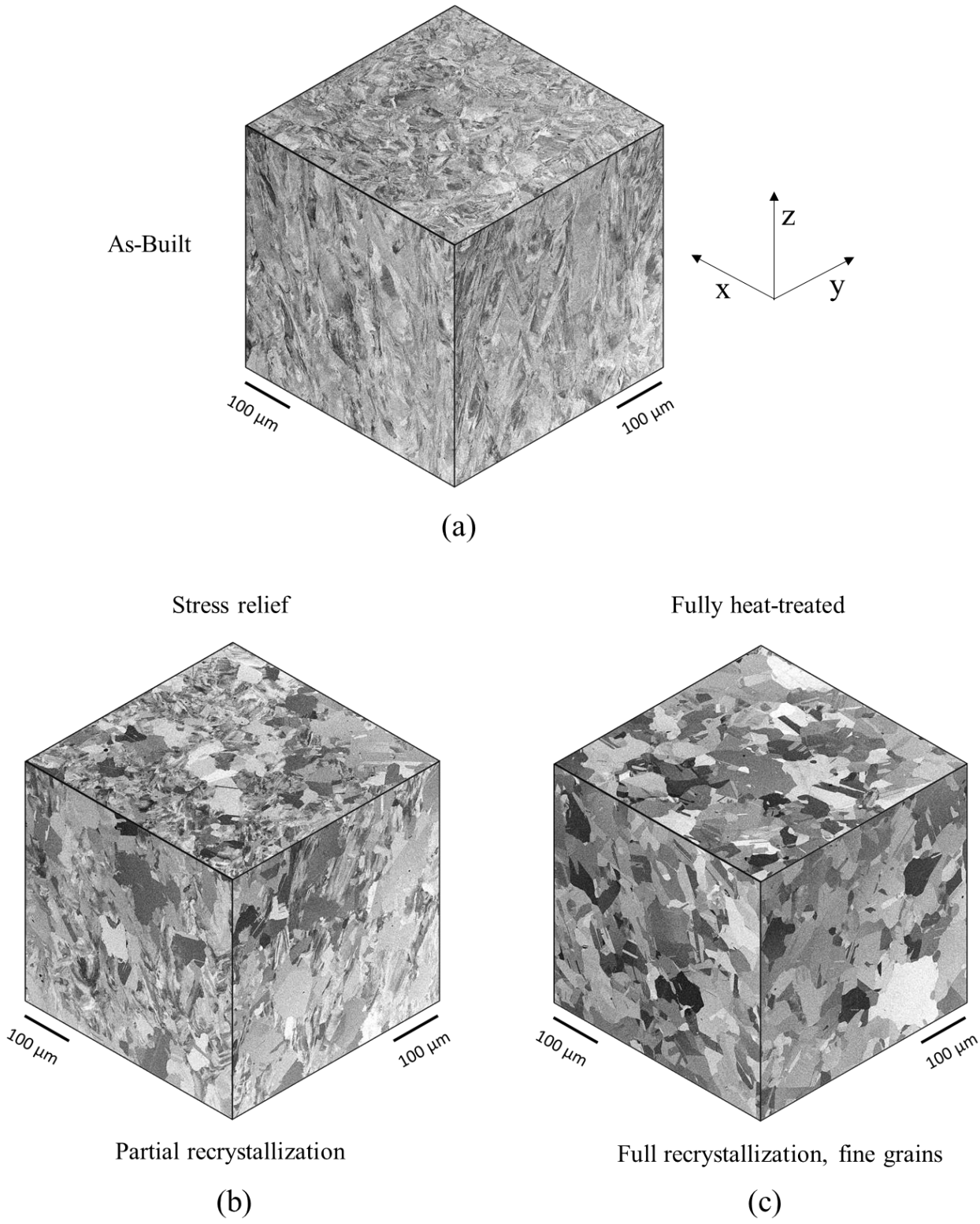


Fig. 14 Quasi-3D images showing microstructure evolution of B-4 samples before and after post-processing heat treatment (formulation II).

Table 4. Summary of tensile properties of L-PBF NASA HR-2 at three temperatures.

Material	Test Environment	Composition	Yield Stress (ksi)	Ultimate Tensile Stress (UTS)	Fracture Elongation (%)	UTS/YS Ratio
L-PBF NASA HR-2	Air, -320 °F	Formulation I	130.46	225.61	39.20	1.73
		Formulation II	114.31	215.15	41.91	1.88
	Air, RT	Formulation I	105.24	165.74	34.76	1.57
		Formulation II	93.89	167.21	37.65	1.78
	Air, 1200 °F	Formulation I	93.56	125.90	20.18	1.35
		Formulation II	85.36	121.68	16.93	1.43

It is significant to note that tensile testing at cryogenic temperatures for L-PBF NASA HR-2 results in simultaneous enhancement of both strength and ductility. The materials with FCC crystal lattice, such as NASA HR-2, are very suitable for cryogenic applications as they have more dislocation slip systems (12 systems) that can assist in absorbing plastic deformation to enhance ductility in extremely cold condition. Many FCC alloys exhibit higher strain hardening capability at cryogenic temperature because the internal energy of atoms is greatly reduced, which hampers the movement of dislocations [7]. Tensile fracture elongation is typically proportional to the value of strain hardening exponent (n) as high strain hardening capability can homogenize plastic deformation and retard tensile fracture initiation (necking). Therefore, the improved ductility in cryogenic temperatures can be attributed to the enhanced strain hardening capability (higher UTS/YS ratio) that increases the ability to absorb plastic deformation and makes deformation more homogeneous and stable prior to fracture.

G. Deformation and Fracture Behavior at Elevated Temperatures.

Crystal lattice expands at elevated temperatures, and the movement of dislocations becomes easier. As a result, the degree of strain hardening decreases considerably (lower UTS/YS ratio) and slip lines become more widely spaced after tensile testing at elevated temperature. Optical microscopy and SEM were performed to observe deformation-induced microstructure evolution near the fracture surface. As shown in Fig. 15, tensile deformation at 1200 °F results in isolated grain boundary cracking near the fracture surface. It is evident that ductility reduction at 1200 °F is caused by a change in the fracture mode from transgranular to partial intergranular fracture. Grain boundaries provide strengthening effects at lower temperatures, but become a weaker link than the matrix at elevated temperatures. As a result, plastic deformation occurred by mixed dislocation slip and grain boundary sliding at 1200 °F, causing some cracks to develop along grain boundaries as shown in Fig. 15. L-PBF NASA HR-2 is recommended for component applications up to 1200°F.

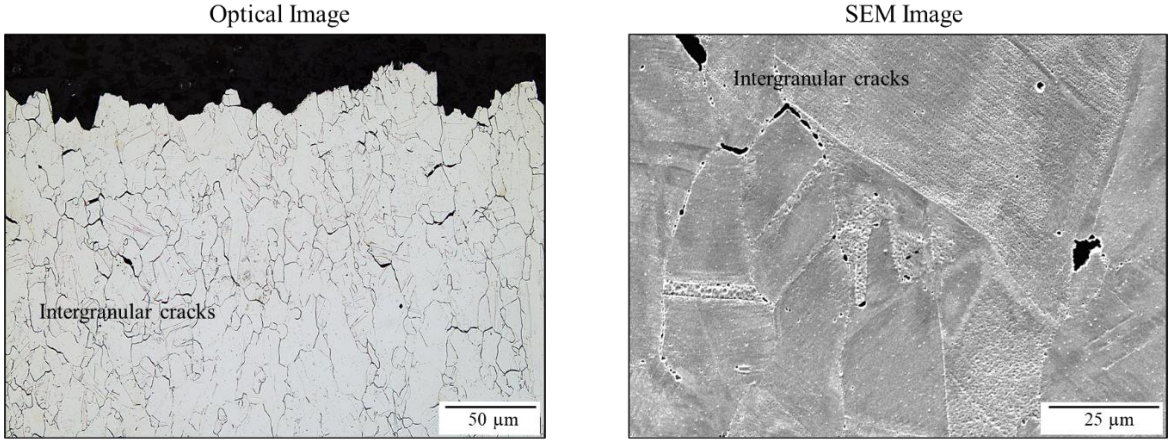


Fig. 15 Cross-sectional views of the fractured tensile samples after testing at 1200 °F.

Fig. 16 presents the fracture surface morphologies of L-PBF NASA HR-2 tensile tested at 1200 °F. The fracture surface displays predominantly ductile transgranular fracture mode. However, several small partial intergranular fracture zones are present near the specimen gauge surface. It is evident that the presence of isolated partial intergranular fracture contributes to the reduction in fracture elongation from 34 - 38% at room temperature to 17 - 20% at 1200 °F. Grain boundaries can become the weakest link when the temperature exceeds 0.5 T_m (melting temperature), which is approximately 1250 °F for L-PBF NASA HR-2 [35]. Plastic deformation tends to occur by mixed dislocation slip and grain sliding when grain boundaries become weaker than grain interior at elevated temperatures. The presence of partial intergranular fracture zones indicates grain boundary sliding became more prominent at 1200 °F, causing some cracks to develop along grain boundaries as shown in Fig. 16.

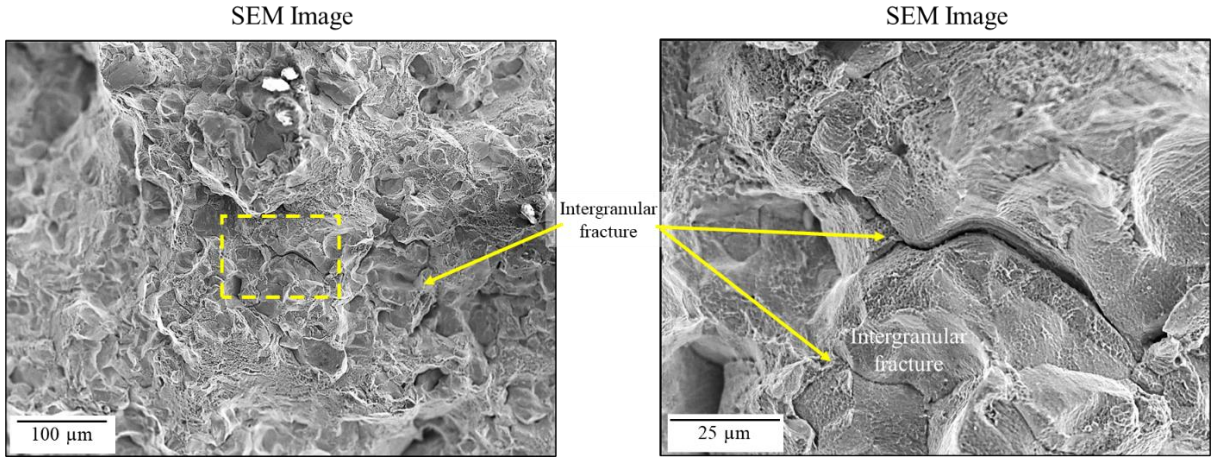


Fig. 16 Fracture surfaces of L-PBF NASA HR-2 tensile tested at 1200 °F. Some isolated partial intergranular fracture zones are present near the specimen gauge surface. Ductile dimple type of fracture predominates away from the specimen gauge surface.

H. L-PBF NASA HR-2 and LP-DED NASA HR-1 Comparison

The tensile properties of L-PBF NASA HR-2 obtained from this study are compared with those of LP-DED NASA HR-1 as reported in the literature [7] and presented in Fig. 17. As shown, the overall correlation of tensile properties and test temperature observed in this study is similar to that observed for LP-DED NASA HR-1. L-PBF NASA HR-2 has higher strength but lower fracture elongation than LP-DED NASA HR-1 under the same test temperatures. Compared with LP-DED NASA HR-1, the ultimate tensile stress of L-PBF NASA HR-2 (formulation II) increases from 202.0 to 225.6 ksi at –320 °F, from 154.0 to 165.8 ksi at room temperature, and from 110.0 to 122.9 ksi at 1200 °F. Although strength decreases with increasing temperature, both yield and tensile strengths remain quite stable up to 1200 °F. Compared with LP-DED NASA HR-1, the ductility of L-PBF NASA HR-2 (formulation II) decreases from 49% to 41.9% at –320 °F, from 41% to 37.7% at room temperature, and from 27% to 16.93% at 1200 °F. Overall, L-PBF NASA HR-2 has slightly lower fracture elongation than LP-DED NASA HR-1, but it is significantly more ductile than most commercial Ni-based and Fe-Ni-based superalloys. L-PBF NASA HR-2 is specifically designed as an AM solution to fabricate hydrogen sensitive components for liquid rocket engine applications. L-PBF NASA HR-2 is also an excellent material for use in extremely cold condition. L-PBF NASA HR-2 exhibits very high ultimate tensile stress of 225.6 ksi and more than 41.0% in fracture elongation at -320 °F, which can be attributed to its enhanced strain hardening capability (higher UTS/YS ratio) at cryogenic temperatures.

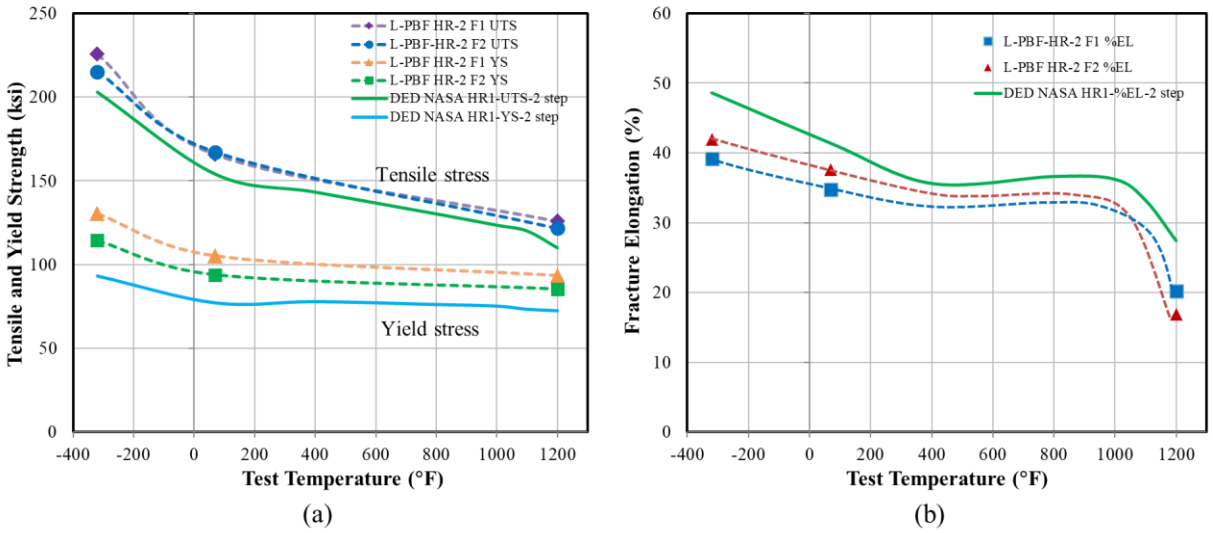


Fig. 17 The tensile properties of L-PBF NASA HR-2 obtained from this study are compared with those of LP-DED NASA HR-1 as reported in the literature [7]: (a) tensile and yield strengths and (b) fracture elongation.

I. Tensile Properties in High Pressure Hydrogen Environment

As the initial material screening to evaluate the susceptibility of hydrogen environment embrittlement (HEE), tensile testing was conducted for L-PBF NASA HR-2 in a 5 ksi high-pressure gaseous hydrogen environment at ambient temperature. The term HEE is used to signify the degradation of certain mechanical properties when the material is exposed to a high-pressure gaseous hydrogen environment as compared to an inert environment [36]. HEE effects are a function of temperature and maximum HEE susceptibility usually occurs near room temperature. The tensile ductility degradation of smooth tensile specimens, tested in hydrogen as compared to that in an inert environment, is commonly used to gauge HEE susceptibility [36]. Fig. 18 shows the microstructure (in X-Z plane) of a L-PBF NASA HR-2 tensile sample prior to tensile testing in hydrogen. Table 5 presents the tensile properties for L-PBF NASA HR-2 tested in 5 ksi gaseous hydrogen at room temperature. All specimens elongated beyond the calibrated extensometer range of 15% strain. Effective elongation is calculated using the initial specimen length, the final fit-back length, and the nominal gage length. As expected, hydrogen has insignificant influence on tensile properties of L-PBF NASA HR-2. Formulation I material exhibits slightly higher yield stress but lower UTS and ductility than the formulation II material. Tensile ductility in hydrogen, as represented by total fracture elongation, ranges from 33.06 -34.80% for formulation I, and from 36.13 – 37.06% for formulation II. It is significant to note that tensile ductility in hydrogen remains quite high for both formulations and is comparable to that in ambient air (see Table 5).

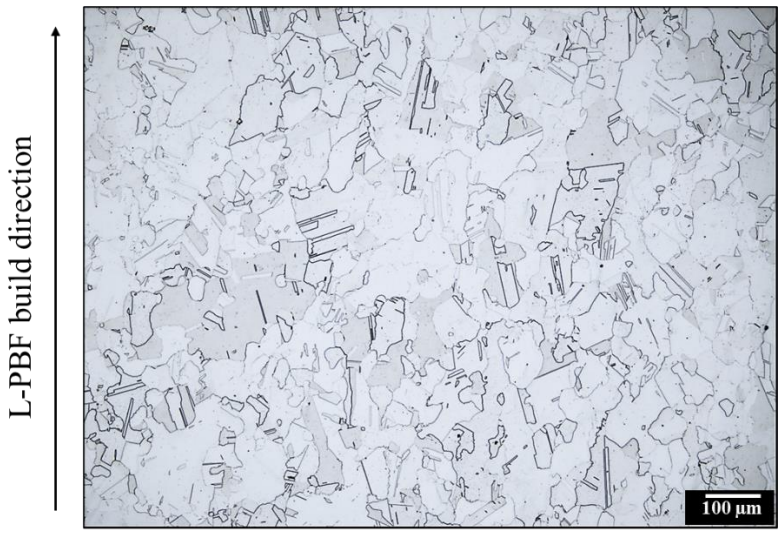


Fig. 18 The typical microstructure (in X-Z plane) of L-PBF NASA HR-2 specimen used for tensile testing in 5 ksi gaseous hydrogen environment. The average grain size is approximately 75 µm.

Table 5. Tensile properties for L-PBF NASA HR-2 in 5 ksi high pressure hydrogen environment.

Material	Strain rate (in/in/min)	Test Environment	Composition	Specimen ID #	Yield Stress (ksi)	Ultimate Tensile Stress (UTS)	Modulus of Elasticity (MSI)*	Fracture Elongation (%)
L-PBF NASA HR-2 (B-4)	0.005	5 ksi GH_2, RT	Formulation I	1-2	95.52	162.72	28.45	33.06
				1-6	97.59	164.76	29.45	34.80
				1-5	95.76	164.69	27.36	34.00
			Formulation II	2-2	90.99	166.06	24.86	37.06
				2-3	91.82	165.57	26.73	36.13
				2-6	92.03	166.23	26.00	36.53

* Modulus of elasticity value is for reference only. Specific modulus tests are required for true value.

The ratios of yield stress (YS), ultimate tensile stress (UTS), and ductility (fracture elongation) for L-PBF NASA HR-2 tested in high pressure hydrogen (GH_2) versus that in air are given Table 6. The most significant effects of high-pressure hydrogen environments are on tensile ductility, notch tensile strength, and crack behavior [20]. The elastic properties and tensile yield stress of metals in hydrogen are generally very close to that in air or inert environments [2,6]. As can be seen in Table 6, The YS ratio for formulation I is unusually low that likely results from the higher-than-expected modulus of elasticity and yield stress for the samples tensile tested in air. Abnormally high modulus of elasticity can occur due to the use of an incorrect type of extensometer. Modulus of elasticity value obtained from tensile testing is for reference only, specific modulus tests are required for true value.

It is significant to note that hydrogen has negligible effect on the ultimate tensile stress as the UTS ratios (GH_2/air) for L-PBF NASA HR-2 are above 99%. This finding indicates that hydrogen had little effect on the stress required to initiate plastic deformation. The primary effect of hydrogen is in general on plastic deformation and ductility. Tensile ductility ratios (GH_2/Air) is widely used to assess the susceptibility of HEE. L-PBF NASA HR-2 exhibits a slight reduction in tensile ductility in hydrogen with ductility ratios (GH_2/air) around 97 to 98% for both formulations as illustrated in Fig. 19. Although L-PBF NASA HR-2 shows very high GH_2/air tensile ductility ratio, tensile properties in hydrogen are intended for the initial material screening and should not be used for component design. Additional mechanical testing in high pressure hydrogen environment is needed to evaluate the effects of hydrogen on other critical mechanical properties such as low cycle fatigue, high cycle fatigue, and fatigue crack growth.

Table 6. The GH_2/air ratios of yield stress (YS), ultimate tensile stress (UTS), and ductility (fracture elongation) for L-PBF NASA HR-2.

Material	Strain rate (in/in/min)	Composition	YS Ratio (GH_2/Air)	UTS Ratio (GH_2/Air)	Ductility Ratio (GH_2/Air)
L-PBF NASA HR-2 (B-4)	0.005	Formulation I	0.92	0.99	0.98
		Formulation II	0.98	0.99	0.97

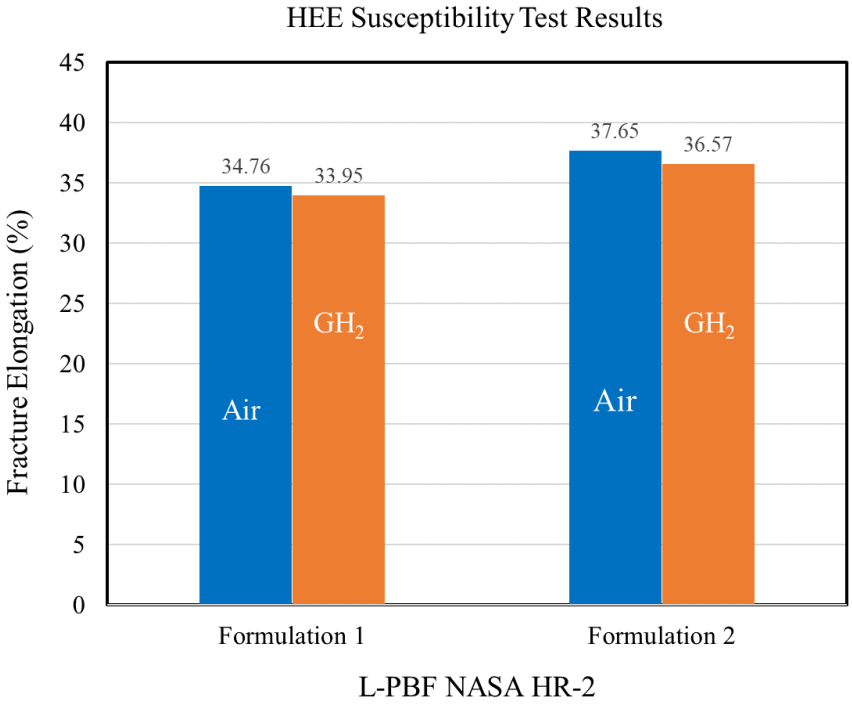
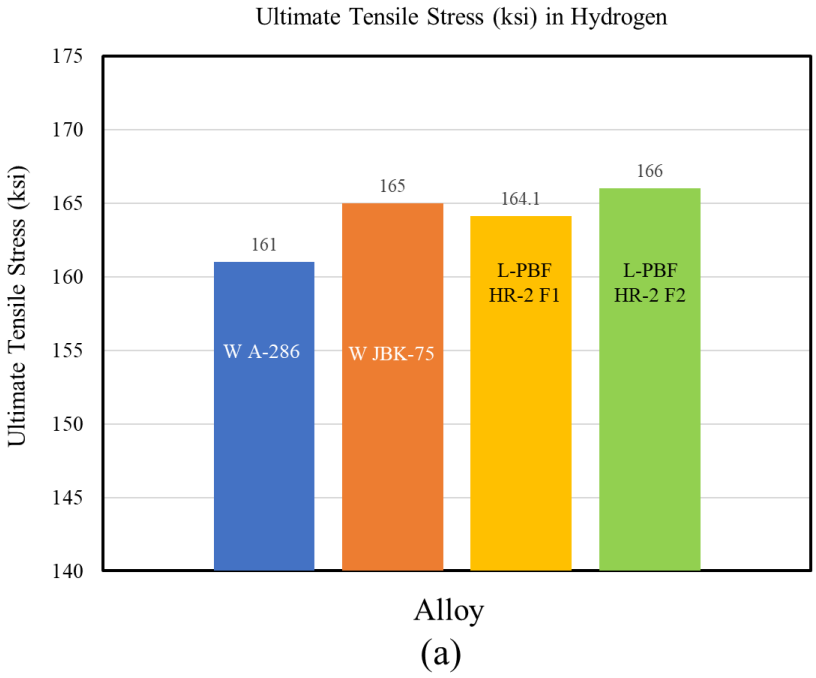


Fig. 19 HEE susceptibility comparison for L-PBF NASA HR-2 formulation I and II (B-4 parameter). Both formulations show a slight reduction in tensile fracture elongation when testing in a 5ksi gaseous hydrogen environment versus that in ambient air.

Alloys A-286 and JBK-75 are well-known HEE resistant Fe-Ni-based superalloys that are being used for hydrogen sensitive components in RS-25 rocket engine. Comparison of tensile properties in hydrogen for wrought A-286, wrought JBK-75, and L-PBF NASA HR-2 are shown in Fig. 20. All three alloys have excellent resistance to HEE and display negligible degradation in UTS and ductility in hydrogen. Comparing with the wrought A-286 and JBK-75 alloys, L-PBF NASA HR-2 exhibits comparable ultimate tensile stress, but significantly higher ductility (fracture elongation) in hydrogen as shown in Fig. 20. The most outstanding attribute of L-PBF NASA HR-2 is that it has high tensile strength of more than 165 ksi (1210 Mpa), while maintaining higher than 34% fracture elongation in hydrogen. Wrought A-286 and JBK-75 have excellent resistance to HEE, but they are not as ductile as L-PBF NASA HR-2 and have lower fracture elongation (22 – 23%) in hydrogen.

Although A-286 and JBK-75 have excellent resistant to HEE, both alloys have limitations as they cannot be readily built using L-PBF. A-286 has poor weldability and JBK-75 is very susceptible to hot cracking during L-PBF process [9,10]. NASA HR-2 was specifically developed as an AM solution for fabricating hydrogen sensitive LRE components that require exceptional resistance to HEE. NASA HR-2 has excellent 3D printability and is the only HEE resistant superalloy that can be built via L-PBF technique. L-PBF has provided new design and manufacturing opportunities for NASA HR-2 to fabricate hydrogen sensitive components that have complex shape and need fine feature resolution. L-PBF NASA HR-2 will be demonstrated for various LRE components targeting hydrogen fuel turbopumps in RS-25 engine for forging and casting replacements.



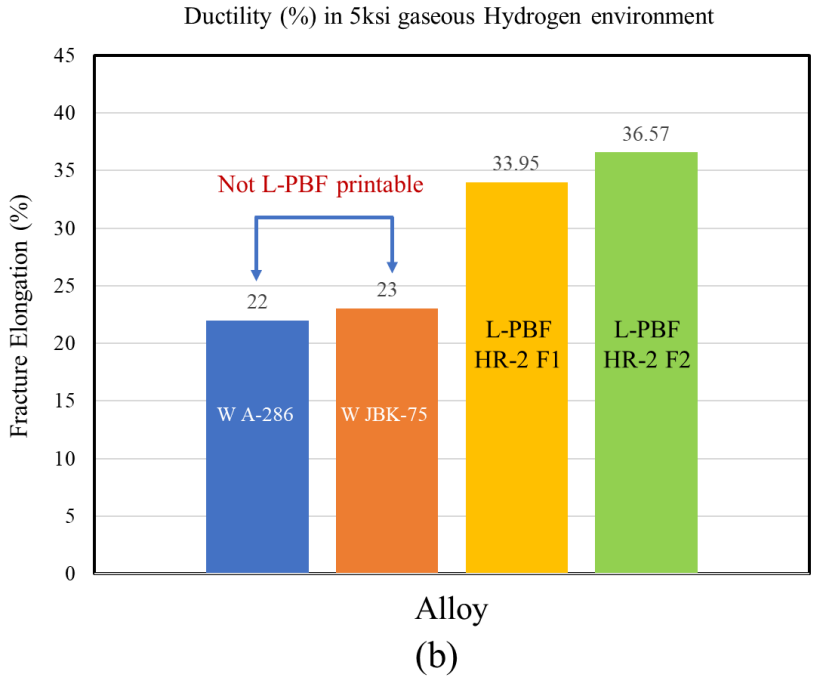


Fig. 20 Comparison of (a) ultimate tensile stress and (b) tensile fracture elongation in hydrogen for wrought A-286, wrought JBK-75, and L-PBF NASA HR-2. A-286 and JBK-75 are not printable via L-PBF. L-PBF NASA HR-2 (B-4 parameter) exhibits comparable ultimate tensile stress, but significantly higher fracture elongation than A-286 and JBK-75 in hydrogen.

J. Effects of Hydrogen on Fracture Behavior

Fracture surfaces were analyzed using SEM to explore the effects of hydrogen on tensile fracture behavior. Fractographic details and tensile failure mode of a formulation II specimen are shown in Fig. 21. Three images are

presented, including a hydrogen affected zone near the surface, and two higher resolution images showing mixed quasi-cleavage and ductile dimple fracture in the hydrogen affected zone. As shown in Fig. 21, the interaction of gaseous hydrogen with the tensile specimen is confined within its outer region. There is a very small hydrogen affected zone around the circumference of the fracture surface. Higher resolution SEM images reveal the hydrogen affected zone has mostly ductile dimple type of fracture with a few very small hydrogen-induced quasi-cleavage cracks. It is apparent that hydrogen has little influence on the tensile fracture behavior of L-PBF NASA HR-2.

The quasi-cleavage fracture zone is very small and mixed with traces of ductile dimples. Outside of the hydrogen affected zones, the fracture surface exhibits predominant ductile dimple type of fracture. Although there is a hydrogen affected quasi-cleavage zone on the fracture surface, L-PBF NASA HR-2 remains very ductile with 34 - 36% fracture elongation after tensile testing in hydrogen. From the fractographic analysis, it is evident that the interaction of external gaseous hydrogen with the tensile specimen is confined near the surface during tensile testing. Hydrogen-induced surface cracks initiated from the specimen gauge surface and grew inward for approximately 100 – 150 µm. Intergranular fracture, which is the most severe form of HEE, is not present on the fracture surface of L-PBF NASA HR-2.

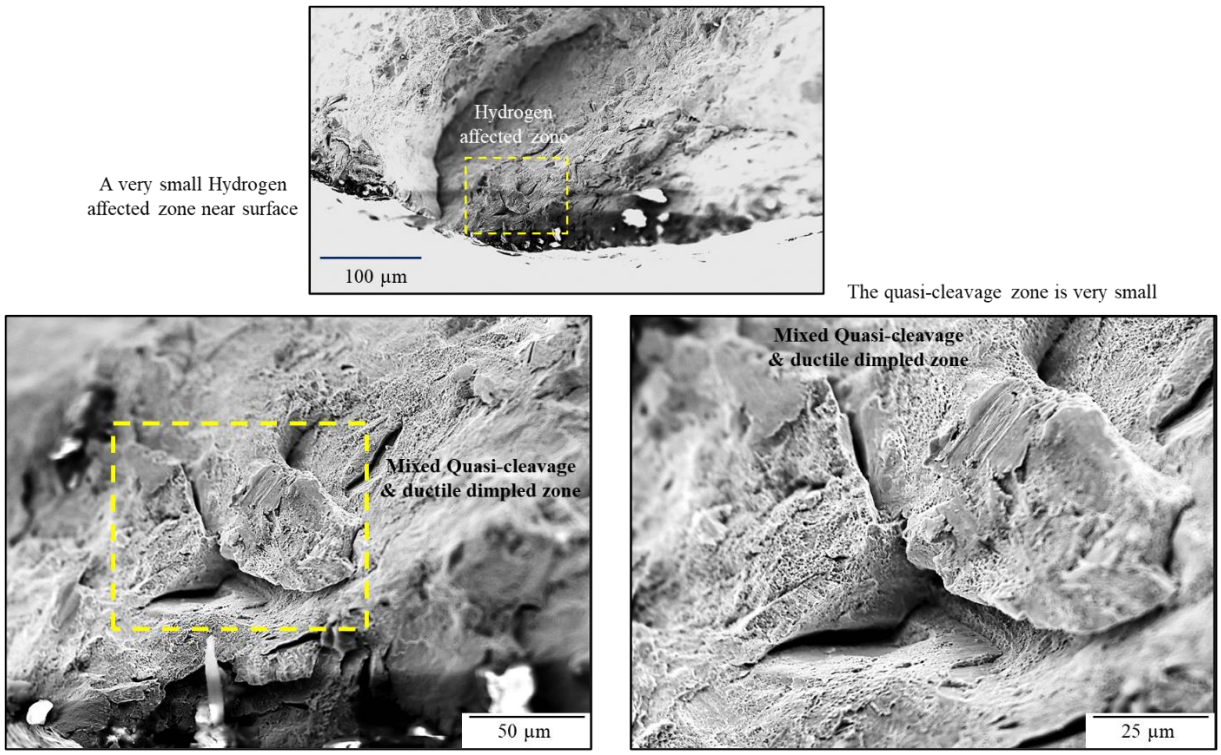


Fig. 21 SEM fractography of a specimen tensile tested in hydrogen showing a very small hydrogen affected zone on the specimen surface. The hydrogen affected zone displays mixed quasi-cleavage fracture and ductile dimpled fracture.

VI. Future Work (Hardware Manufacturing)

L-PBF NASA HR-2 has been demonstrated for its excellent printability and resistance to HEE using an EOS M100 system at Marshall space Flight Center. The development of L-PBF NASA HR-2 will continue using a mid-sized EOS M290 system to print larger samples and demonstration hardware. Tensile properties of the samples built with the M290 will be re-evaluated in hydrogen and in ambient air at various temperatures to compare the effects of switching from the M100 to a M290 system. Heat treatment options will be explored to increase the yield stress to 100 ksi or greater with minimum reduction in ductility. Other critical mechanical property data such as high cycle fatigue (HCF) and low cycle fatigue (LCF) will be generated to ensure L-PBF NASA HR-2 can meet the fatigue life requirements for hydrogen sensitive components in liquid rocket engines. Demonstration hardware will be fabricated using the

M290 system to investigate the design limits for certain specific part features and explore the full potential of L-PBF NASA HR-2. Significant schedule and cost savings will be demonstrated targeting hydrogen-sensitive components that have complex shape and fine feature. The components to be demonstrated include turbine wheel, pump shaft, turbine rotators, turbine nozzle, turbine stator, and other pressure loaded components used in the low pressure hydrogen fuel turbo pump (LPFTP) of the RS-25 rocket engine.

VII. CONCLUSIONS

1) NASA HR-2 is an AM Ni-Fe-based superalloy specifically designed for liquid rocket engine components that need resistance to hydrogen environment embrittlement (HEE). The development of L-PBF NASA HR-2 has advanced through process development, material characterization, and mechanical testing in hydrogen and in ambient air across a range of temperatures. NASA HR-2 manufactured via the L-PBF process is defect free and have the desirable microstructure and tensile properties.

2) The AM feasibility of NASA HR-2 alloy has been demonstrated via the L-PBF technique. NASA HR-2 has excellent printability and can be readily built using L-PBF. Its microstructure evolves well after heat treatment into the desirable highly recrystallized structure with very fine grain size. Its chemical composition was formulated to obtain an optimal balance between HEE resistance, printability, strength, ductility, oxidation resistance, and microstructure evolution after heat treatment. The optimized nominal composition is shown below:

Alloy	Fe	Ni	Cr	Mo	W	Co	Ti	Al
L-PBF NASA HR-2	30.00	41.50	15.50	3.00	3.20	4.00	2.80	0.25

3) L-PBF NASA HR-2 has excellent resistance to HEE as it has high ultimate tensile stress and remains very ductile with more than 34% fracture elongation after tensile testing in hydrogen. The tensile data confirms hydrogen has little influence on its tensile properties and fracture behavior. L-PBF NASA HR-2 is a promising option for many hydrogen sensitive LRE components that need exceptional resistance to HEE. L-PBF NASA HR-2 also has excellent tensile properties in extremely cold environments. Its tensile properties are significantly enhanced in cryogenic condition at - 320 °F (in liquid nitrogen).

4) NASA will continue to advance L-PBF NASA HR-2 and demonstrate its potential of significant cost and schedule savings. Demonstration hardware will be fabricated to investigate the design limits for certain specific part features and explore the full potential of L-PBF NASA HR-2. The components to be demonstrated include turbine wheel, pump shaft, turbine rotators, turbine nozzle, turbine stator, and other pressure loaded components used in the low pressure hydrogen fuel turbo pump (LPFTP) of the RS-25 rocket engine. Other critical mechanical property data such as high cycle fatigue (HCF) and low cycle fatigue (LCF) will be generated to ensure L-PBF NASA HR-2 can meet the fatigue life requirements for hydrogen sensitive components in liquid rocket engines.

Acknowledgments

The authors would like to acknowledge the Mechanical Test team (EM22) that includes Keith Hastings, Jacob Faulk, Matthew Jackson, and Alisson Peusch. The EM22 team members performed tensile tests in 5 ksi high pressure gaseous hydrogen environment, in cryogenic condition, and at elevated temperatures. Tensile property data was provided in a timely fashion to allow for clear and decisive direction on the development of L-PBF NASA HR-2. The authors also acknowledge the powder quality analysis work of Justin McElderry (EM22), and surface quality analysis work of Matthew Mazurkivich (EM22).

References

[1] Gradl, P.R., Mireles, O.R., Katsarelis, C.C., Smith, T.M., Sowards, J.W., Park, A.M., Chen, P.S., Tinker, D.C., Protz, C.S. Teasley, T.W., Ellis, D.L., Kantzos, C.A. “Advancement of extreme environment additively manufactured alloys for next generation space propulsion applications,” Acta Astronautica 211 (2023) 483–497. doi: 10.1016/j.actaastro.2023.06.035

[2] Chen, P.S.; Panda B.; and Bhat, B.N.: "NASA HR-1, A New Hydrogen Resistant Fe-Ni Base Superalloy," *Proc. of the Fifth International Conference on the Effect of Hydrogen on the Behavior of Materials*, The Minerals, Metals and Materials Society, Moran, WY, 1996, pp. 1011–1020
doi: 10.1002/9781118803363.ch89
[3] Chandler, W. T. "Hydrogen-Environment Embrittlement and Its Control in High Pressure Hydrogen/Oxygen Rocket System," Advanced Earth-to-Orbit Propulsion Technology of NASA Conference Publication 2437, no. 2, (1986).
[4] Katsarelis, C.C., Chen, P.S., Gradl, P.R., Protz, C.S, Jones, Z., Ellis, D.L., Evans, L. "Additive Manufacturing of NASA HR-1 for Liquid Engine Component Applications", JANNAF, (December 2019) United States.
[5] Chen, P.S.; Katsarelis, C.C.; Medders, W.M.; and Gradl, P.R.: "Segregation Evolution and Diffusion of Titanium in DED NASA HR-1", NASA/TM 20210013649, May 2021.
[6] Gradl, Paul R., Thomas W. Teasley, Christopher S. Protz, Colton C. Katsarelis, and Po-Shou Chen. "Process Development and Hot-fire Testing of Additively Manufactured NASA HR-1 for Liquid Rocket Engine Applications," AIAA Propulsion and Energy Forum (2021).
doi: 10.2514/6.2021-3236
[7] Chen, P.S., Katsarelis, C.C, Medders, W.M., Gradl, P.R., Su, C.H. "Development of Directed Energy Deposited NASA HR-1 to Optimize Properties for Liquid Rocket Engine Applications," NASA/TM 20230006075, April 2023.
[8] Chen, P.S., Fullen, M.D., Watwood, W.C., Rupp, B.L., Medders, W.M, Colton, C.C., Gradl, P.R. "Effects of Strain Rate and Surface Finish on Tensile Properties in High Pressure Hydrogen - A Case Study for LP-DED NASA HR-1," NASA/TM 20230008831, June 2023.
[9] Brooks, J.A., Krenzer, R.W, "Progress Toward a More Weldable A-286," Welding Research Supplement, p. 242-245, June 1974.
[10] L-PBF JBK-75 Development, Internal Research, NASA Marshall Space Flight Center, AL.
[11] Morinaga, M., Yukawa, N., Ezaki, H., and Adachi, H., "Solid Solubilities in Transition-Metal-Based f.c.c. Alloys." Philosophical Magazine A, Vol. 51, No. 2, pp. 223–246, 1985.
doi: 10.1080/01418610.1985.12069159
[12] Morinaga, M., Murata, Y., and Yukawa, H., "Recent Progress in Molecular Orbital Approach to Alloy Design," 2004.
doi: 10.4028/www.scientific.net/msf.449-452.37
[13] Morinaga, M., and Yukawa, H., "Alloy Design with the Aid of Molecular Orbital Method." Bulletin of Materials Science.
doi: 10.1007/BF02747420, 1997.
[14] Morinaga, M., Yukawa, N., and Adachi, H., "Alloying Effect on the Electronic Structure of Ni3Al (γ′)," Journal of the Physical Society of Japan, Vol. 53, No. 2, pp. 653–663, 1984.
doi: 10.1143/jpsj.53.653
[15] Morinaga, M., Yukawa, N., Adachi, H., and Ezaki, H., "Superalloys," E.A. Loria (eds), The Minerals, Metals & Materials Society, Warrendale, PA, pp. 523–532, 1984.
[16] Morinaga, M., Yukawa, N., and Adachi, H., "Alloying effect on the electronic structure of BCC Fe," Journal of Physics F: Metal Physics, Vol. 15, No. 5, pp. 1071–1084, 1985.
doi: 10.1088/0305-4608/15/5/012
[17] Lee, J.A., "Effects of the Density of States on the Stacking Fault Energy And Hydrogen Embrittlement of Transition Metals And Alloys," Effects of Hydrogen on Materials Proceedings of the International Hydrogen Conference, B. Somerday, P. Sofronis, R. Jones, (eds.), pp. 678–685, 2008.
[18] Toyoda, K., Fujita, H., Sawatari, H., and Yoshida, K., "Effect of Stacking Fault Energy on Recrystallization in Cold Worked FCC Crystals", Transactions of the Japan Institute of Metals, Vol. 25, No. 5 (1984), pp. 339 to 347.
doi: 10.2320/matertrans1960.25.339
[19] Özbilen, S., "Satellite formation mechanism in gas atomised powders," Powder Metallurgy 42(1):70-78, January 1999.
doi: 10.1179/pom.1999.42.1.70
[20] Keshavarzkermani A., Esmaeilizadeh, R., Ali, U., Enrique, P.D., Mahmoodkhani, Y., Zhou, N.Y., Bonakdar, A., Toyserkani, E., "Controlling mechanical properties of additively manufactured hastelloy X by altering solidification pattern during laser powder-bed fusion," Materials Science & Engineering A 762 (2019) 138081.
doi: 10.1016/j.msea.2019.138081
[21] Hibino S., Fujimitsu K., Azuma M., Ishimoto T., and Nakano T., "Effects of Recrystallization on Tensile Anisotropic Properties for IN738LC Fabricated by Laser Powder Bed Fusion," Crystals 2022, 12, 842.
doi: 10.3390/cryst12060842.
[22] Konstantinos, G., Khan, R., and Kartal, M.E.," The influence of pulsed laser powder bed fusion process parameters on Inconel 718 material properties," Materials Science & Engineering A 769 (2020) 138527.
doi: 10.1016/j.msea.2019.138527
[23] Kumar, P., Farah J., Akram, J., Teng, C., Ginn, J., Misra, M.," Influence of laser processing parameters on porosity in Inconel 718 during additive manufacturing," The International Journal of Advanced Manufacturing Technology (2019) 103:1497–1507.
doi: 10.1007/s00170-019-03655-9
[24] Robinson, J.H., Ashton I.R.T., Jones, E., Fox, P., and Sutcliffe, C., "The effect of hatch angle rotation on parts manufactured using selective laser melting," Rapid Prototyping Journal, 25/2 (2019) 289–298, Emerald Publishing Limited [ISSN 1355-2546].

doi: 10.1108/rpj-06-2017-0111
[25] Obeidi, M.A., "Metal additive manufacturing by laser-powder bed fusion: Guidelines for process optimization," Results in Engineering 15 (2022) 100473.
doi: 10.1016/j.rineng.2022.100473
[26] Li, L., Anand, S., "Hatch Pattern Optimization of Powder Bed Fusion Additive Manufacturing process for minimizing flatness error," Procedia Manufacturing 53 (2021) 456–465.
doi: 10.1016/j.promfg.2021.06.049
[27] Sames, W.J., List, F.A., Pannala, S., Dehoff, R.R., Babu, S.S.," The metallurgy and processing science of metal additive manufacturing," International Materials Reviews Volume 61, 2016 - Issue 5.
doi.org: 10.1080/09506608.2015.1116649
[28] Adomako N.K., Haghdadi, N., Primig, S.," Electron and laser-based additive manufacturing of Ni-based superalloys: A review of heterogeneities in microstructure and mechanical properties," Materials & Design 223 (2022) 111245.
doi: 10.1016/j.matdes.2022.111245
[29] Fencheng, L., Xin, L., Gaolin, Y., et al., "Recrystallization and its influence on microstructures and mechanical properties of laser solid formed nickel base superalloy Inconel 718," Rare Metals, Vol. 30, No. 1, pp. 433–438, doi:10.1007/s12598-011-0319-0, March 2011.
doi: 10.1007/s12598-011-0319-0
[30] Zhang, F., Levine, L.E., Allen, A.J., et al.: "Effect of heat treatment on the microstructural evolution of a nickel-based superalloy additive-manufactured by laser powder bed fusion," Acta Materialia, Vol. 152, pp. 200–214, June 2018.
doi: 10.1016/j.actamat.2018.03.017
[31] Cao, J., Liu, F., Lin, X., et al.: "Effect of overlap rate on recrystallization behaviors of Laser Solid Formed Inconel 718 superalloy," Optics & Laser Technology, Vol. 45, pp. 228–235, February 2013.
doi: 10.1016/j.optlastec.2012.06.043
[32] Hibino S., Fujimitsu K., Azuma M., Ishimoto T. and Nakano T.," Effects of Recrystallization on Tensile Anisotropic Properties for IN738LC Fabricated by Laser Powder Bed Fusion," Crystals 2022, 12, 842.
doi: 10.3390/cryst12060842.
[33] Weaver, J.S., Rosenthal, I.," Understanding Anisotropic Tensile Properties of Laser Powder Bed Fusion Additive Metals: A Detailed Review of Select Examples," NIST Advanced Manufacturing Series 100-44.
doi: 10.6028/NIST.AMS.100-44.
[34] Nandy, S., Sekhar, A.P., Kar, T., Ray, K.K., and Das, D.: "Influence of ageing on the low cycle fatigue behaviour of an Al–Mg–Si alloy," Philosophical Magazine,
doi: 10.1080/14786435.2017.1322729, 2017.
[35] Saravanan, K.; Chakravadhanula, V.S.K.; Manwatkar, S.K.; Narayana, S.V.S.; and Narayanan, P.R.: "Dynamic Strain Aging and Embrittlement Behavior of IN718 During High-Temperature Deformation," Metallurgical and Materials Transactions, Vol. 51A, pp. 5691–5703, November 2020.
doi: 10.1007/s11661-020-05970-3
[36] Lee, J.A., "Hydrogen Embrittlement", NASA Technical Memorandum, 2016-218602.